

Interpretation of detailed density profiles of alpine ice cores as past environment proxy signal

KANAMORI Syosaku

Ph. D. Dissertation

Graduate School of Environmental Science
Hokkaido University
March 2008

Contents

Contents	1
1. Introduction	3
1.1. Temporal resolution in ice core studies	3
1.2. Density profiles of ice cores	4
1.3. Objectives of this study	6
2. Ice coring, field measurements and ice core measurements.....	8
2.1. Ice coring	8
2.2. Spatial distribution of annual accumulation rate at the Summit Caldera, Mt. Wrangell	14
2.3. Accumulation measurements for individual storms on Mt. Wrangell.....	14
2.4. Density measurements.....	20
3. Interpretation of detailed density profiles at Mt. Wrangell	29
3.1. Relationship between surface condition and density profile.....	29
3.2. Effect of densification on detailed density profiles	34
4. Detailed dating of Mt. Wrangell cores.....	37
4.1. Estimation of surface condition at Mt. Wrangell from weather station data....	37
4.2. Detailed dating of the Mt. Wrangell ice cores	43
4.3. Monthly variation of parameters in ice core data	50
5. Effect of snow drift at alpine ice core sites	56
5.1. Comparison of annual accumulation rates	56
5.2. Effect of erosions to ice core parameters.....	60
5.3. Bending in depth-density profile	62
5.4. Redistribution of accumulated snow at the Summit Caldera of Mt. Wrangell.	63

6. Conclusions	66
6.1. Interpretation of detailed density profiles as past surface condition proxy data	
66	
6.2. Detailed dating using density profiles	66
6.3. Accumulation environment of alpine ice core sites.....	67
6.4. Meaning of this study	67
Reference	69
Appendix A Detection of snow burial dates at the snow accumulation measurement ...	73
June 2005	73
July 2005	74
August 2005.....	76
September 2005	80
October 2005	81
November 2005	83
December 2005.....	84
January to May 2006	86
Appendix B.....	88
Acknowledgements	91

1. Introduction

1.1. Temporal resolution in ice core studies

Ice core studies unveil past climate history with various timescales. Ice cores from the Greenland ice sheet or Antarctic ice sheet date back to past hundreds thousands years covering glacial and interglacial cycle [e.g. Dansgaard et al., 1993; Greenland Ice-core Project Members, 1993; Petit et al., 1999]. Annual layer thicknesses are thin in such polar ice cores. For example, annual layer thicknesses in Dome Fuji ice core, which is one of the oldest ice cores was less than 40 mm in ice thickness (Watanabe et al., 1999). Alpine ice cores from high accumulation sites cover ice for hundreds years, which enable to reconstruct El Niño-Southern Oscillation Events (ENSO) or Pacific Decadal Oscillations (PDO) [e.g. Thompson, 1984; Kang, 2005]. Annual layer thickness are thick in such mountain ice cores. For example, annual layer thicknesses in Mt. Wrangell ice core where is located in south central Alaska were a few meters in ice equivalent. Such ice cores have higher potential for analysis with high temporal resolution.

The highest time resolution in dating ice core was annual to seasonal ones. Schwikowski et al. [1999], for example, dated an ice core from Fiescherhorn glacier, Swiss Alps using annual layer counting of seasonally changing parameters such as tritium or stable isotope ratio. Nakazawa et al. [2005] determined four seasonal layers using various species of pollen grains at Belukha glacier in Russia's Altai Mountains. In such alpine sites, surface melting events, episodic precipitation, wind erosion and snow drift make dating of ice core difficult and high temporal resolution is scarcely detained..

Analysis of ice core with higher temporal resolution as precise as monthly

scale enlarges the potential of ice core study; one of the advantages of ice cores as past climate proxy is that ice core contains past transported materials in atmosphere such as Kosa dust (e.g. Goto-Azuma et al., 2003) which comes by episodic events. The dating with monthly time scale makes it possible to examine such events with a help of atmospheric observations and/or model results and helps understanding of interactions to climate- or eco-systems. The combined analysis based on monthly scale dating of an ice core also helps understanding of other ice core parameters such as stable isotope ratio.

The key factors which limit temporal resolution of ice core dating are variation of accumulation rate caused by episodic precipitation events, wind erosion and snow drift. Although effect of melting is also the problem for ice core dating, this can be avoided by site selection in the case of alpine glaciers at high latitude, which is the target of this thesis. The author focused detailed density profile to examine amount of accumulation in each event which is affected by episodic precipitation event, wind erosion and snow drift. At a snow surface, textures and density depends on conditions during and after the accumulation (Akitaya and Yamada, 1991). In detail, shapes of precipitated snow crystals and weather conditions changes snow densities in the accumulation event. Temperature and overburden pressure changes snow densities after the accumulation event. Hence, detailed density profile of ice core reflects history of surface condition directly.

1.2. Density profiles of ice cores

At glaciers with dry snow facies, density monotonically increases with depth by densification processes in broad view. At the first stage of densification, where

density is less than 550 kgm^{-3} , mechanical packing of ice grains dominates the densification process. The second stage, where density is $550\text{-}730 \text{ kgm}^{-3}$, densification process occurs by the mechanical packing and plastic deformation of ice grains. At the third stage, where density is $730\text{-}820$ or 840 kgm^{-3} which close off air bubbles, plastic deformation dominates the densification process. At the fourth stage, where density is higher than the close off density, shrinkage of the air bubble dominates the densification process [Maeno and Kuroda, 1986].

In conventional volumetric density measurement for the ice core, resolution was 0.5-1.0 m along core length because it depends on length of each core pieces. This is too coarse to detect density variations caused by intra-annual accumulation events. Density measurement methods using gamma ray or X-ray dramatically improved the resolution of measurement. Gerland et al. [1999] non-destructively measured density profile of 181m-long ice core from Berkner Island, Antarctica using gamma ray. The resolution was 3mm along core length and the absolute accuracy was 2%. Hori et al. [1999] measured density profile of Dome Fuji ice core using X-ray. The resolution was 1mm along core length and the absolute accuracy was 1%. Both of the density profiles show that density fluctuations in millimeter scale were maintained through densification process. Although variations of density disappear at deeper part in the fourth stage of densification processes, the record remains at least in the firn part. The age of firn part differs from site to site by local condition; it is almost determined by accumulation rate and temperature empirically [Herron and Langway, 1980].

In pit studies at glacier surface, seasonal variation of density has been examined. In Greenland, typical summer layer is coarse grained and low-density layers and typical winter layer is relatively fine grained, homogeneous and high-density.

Summer layers has more variability than winter layer in stratigraphy and density [Benson, 1962]. On the other hand, Koerner [1971] reported summer layer was denser at the Plateau station in Antarctica. Density profiles reflect local accumulation condition and the characteristics of the density profiles at the surface vary from place to place.

Zwally and Li [2002] explained seasonality in density profile and seasonality of surface elevation at the summit of Greenland by seasonality of densification rate. Gerland et al. [1999] found that denser tendency in winter layer at shallower part inversed at deeper part in the density profile of Barkner Island core, Antarctica. Hence, density profile of ice core can reflect not only surface conditions but also densification process. Both effect should be considered in interpretations of density profiles.

1.3. Objectives of this study

The main purpose of this study is to read climatic and/or environmental histories with the highest temporal resolution from ice cores to connect ice core data and observed data and/or model data in timing. An alpine glacier filling the Summit Caldera of Mt. Wrangell, Alaska (62°N , 144°W ; 4100 m a. s. l.) was selected as the ice coring site because high accumulation rate of $2.5 \text{ m w. e. a}^{-1}$ allows analysis with high temporal resolution.

Three objectives were pursued in the thesis. The first objective is to interpret detailed density profiles of ice cores as a past accumulation event proxy data. In situ accumulation measurement at the Summit Caldera of Mt. Wrangell and detailed density profiles of ice cores with millimeter scale at the corresponding period were compared to establish the relationship between the surface conditions and characteristics of the density profile at the surface layers. Then density variations through densification

process were examined by comparison with density profiles before and after the densification.

The second objective is to date the Mt. Wrangell ice core with monthly time scale. The result of in situ accumulation measurement at the Summit Caldera of Mt. Wrangell was correlated to precipitation and temperature data at regional weather stations which can date back to early 20th century. Then surface events at the Summit Caldera of Mt. Wrangell which formed characteristic features in the density profiles at deeper part were connected with correlated events in regional weather data and the density features were dated by the timing of the correlated events in the regional weather data.

The third objective is to evaluate accumulation environment of alpine ice core drilling sites to understand condition of the sites for the analysis with high time resolution. Windy weather is expected at high mountain sites. For example, weather meter at 5770 m a. s. l. near the Summit of Mt. McKinley was often destroyed after winter season because of windy storms [Okura, personal commun.]. Areas with bared rocks in glaciers which are often seen at mountain sites suggest precipitated snow isn't caught there. Saddle locations or ice caps are often selected as drilling sites in mountain sites because they tend to have relatively thick ice and gentle surface which imply older record with less effect of glacier flow. But such locations would have windy weather and would be affected by wind erosions or snow drift. The King Col, Mt. Logan is one of typical alpine ice core sites located at a saddle in high elevation. Detailed density profile and accumulation time series at the King Col is examined in this context to evaluate condition of a typical alpine ice core site.

2. Ice coring, field measurements and ice core measurements

2.1. Ice coring

2.1.1. Ice core sites

Ice cores were drilled at two sites, which have different characteristics in topography in the Wrangell-St. Elias Mountains. One is the Summit Caldera, Mt. Wrangell (62°N , 144°W ; 4100 m a. s. l.) [Shiraiwa et al., 2004] and the other is King Col, Mt. Logan (61°N , 141°W ; 4135 m a. s. l.) [Goto-Azuma et al., 2003; Shiraiwa et al., 2003] (Fig. 2.1). These areas are extend into the dry snow facies [Benson, 1968; Partington, 1998] and there is no significant melting higher than 4000 m approximately. Several ice cores have been obtained from this region to study past climate [Benson, 1984; Fisher et al., 2004; Goto-Azuma et al., 2003; Holdsworth et al., 1992; Shiraiwa et al., 2004; Yalcin et al., 2006; Zagorodnov et al., 2005; Fig. 2.1]. The Summit Caldera of Mt. Wrangell is unique in topography. The ice filled caldera at the summit is like a bowl gathering snow. Such caldera filled by aged ice is rare and number of the reports of ice coring in a caldera is limited [e.g. Shiraiwa et al., 2001]. On the other hand, saddle location of King Col, Mt. Logan is one of typical sites in alpine ice coring. Ice core sites shown in Figure 2.1 are all located at saddle except Mt. Wrangell and Eclipse Ice Field. Flat surfaces and relatively thick ice, which are important prerequisites for ice coring because effect of glacier flow is small and older ice can be extracted, are found in saddle locations often. Detailed density profiles were examined at Mt. Wrangell carefully then compared with the King Col data.

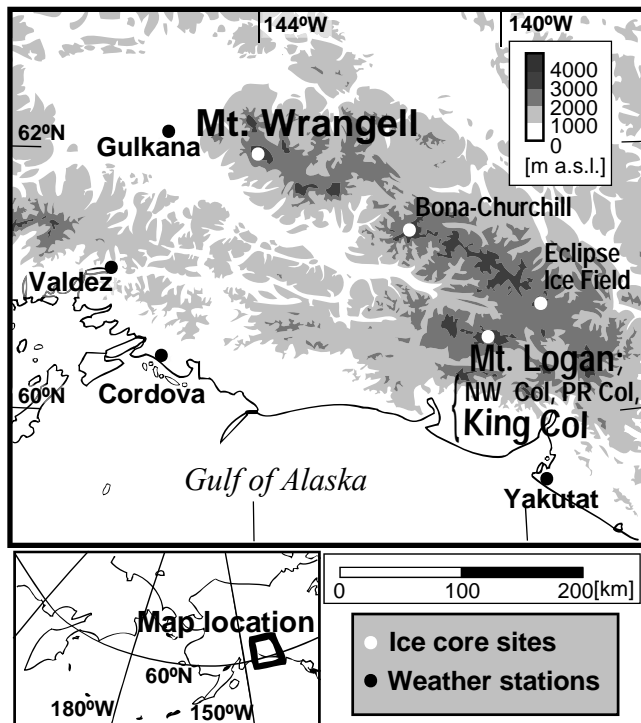


Figure 2.1: Map of the Wrangell-St.Elias Mountains showing the location of ice coring site at Mt. Wrangell (4100 m), King Col (4135 m) , other ice core sites and weather stations. The ice core sites in the map include Northwest Col (5340 m) and Prospector-Russell Col (5340 m) in Mt. Logan, Eclipse Ice Field (3017m) and Bona-Churchill (4400m).

2.1.2. The Summit Caldera, Mt. Wrangell

Mt. Wrangell has a broad summit area of more than 35 km^2 above 4000 m altitude and is dominated by a large $4 \times 6 \text{ km}$ ice-filled Summit Caldera with post-caldera craters along its rim (Fig. 2.2). Most of ice in the Summit Caldera is drained through Long glacier at the south side. Various glaciological and volcanological studies have been conducted by Carl Benson and his colleagues from 1960s on Mt. Wrangell [e.g. Benson and Mothyka, 1978; Benson et al., 2007]. The 10 m-deep temperatures at the Summit Caldera were $-20 \pm 0.5^\circ\text{C}$ in the 1960s and in 1976 [Benson and Motyka, 1978] and -18.9°C in a recent study [Shiraiwa et al., 2004]. Snow cover at the Summit Caldera is slightly below the dry snow line [Benson, 1968] and a few ice

lenses which have several millimeter thick were found in most of annual layers. Benson obtained 44m-deep ice core at north rim of the Summit Caldera in 1982 [Benson, 1984]. This is the longest and the best dated ice core among Benson's works. New seven ice cores were obtained at the Summit Caldera from 2003 to 2006 as the author describe later. The ice thickness is thought to exceed 900 m, but a definite bottom has not yet been detected [Clarke et al., 1989; Benson et al., 2007]. The deepest ice core, which was 216 m-deep and drilled in 2004 didn't reach the bedrock.

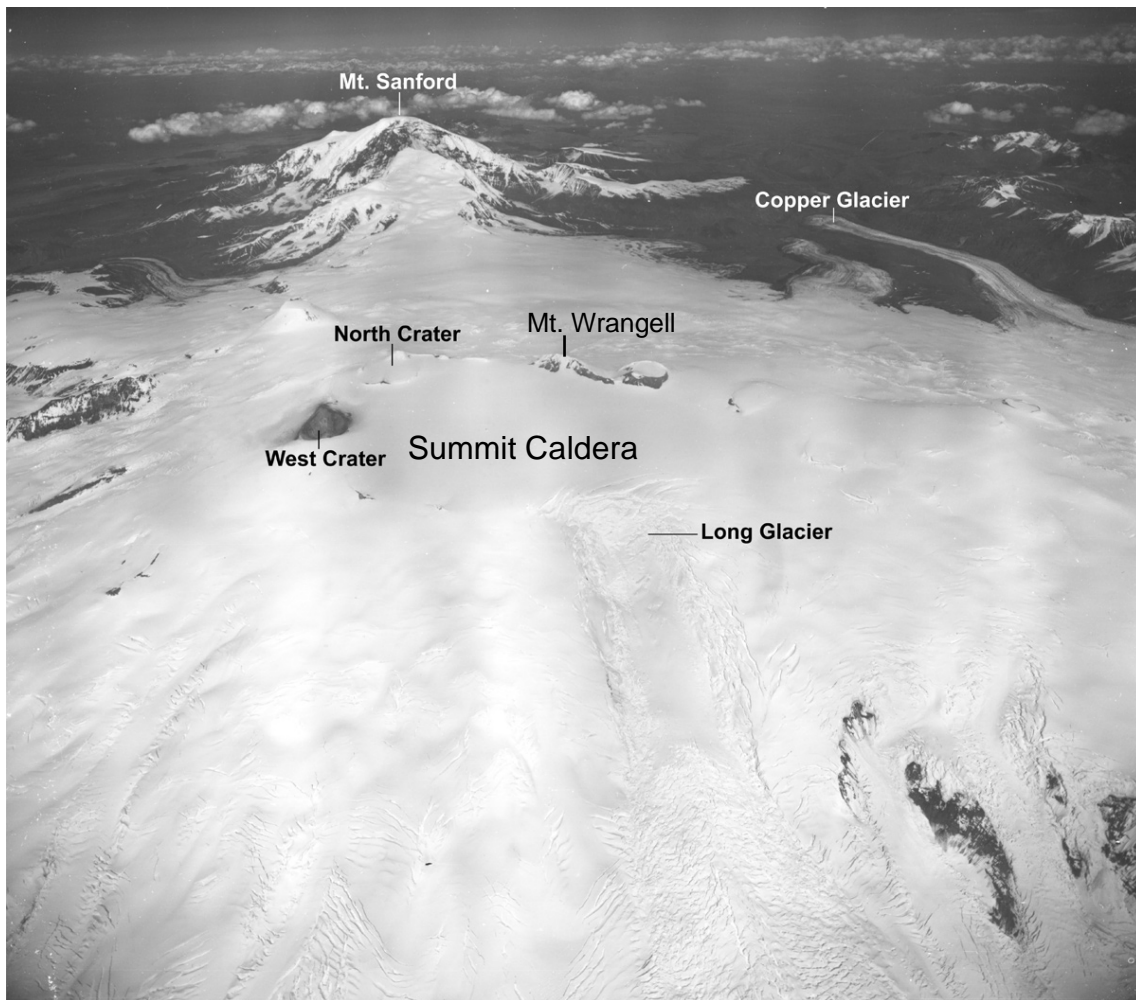


Figure 2.2: Aerial photograph of Mt. Wrangell (4317m) from the south, with Mt. Sanford (4950m) taken by the US Air Force for the USGS in 1948. Original photograph was presented by Benson et al. [2007].

Detailed density measurements were carried out for five new ice cores. The drilled depth, year, and location of each core is shown in Table 2.1 and Figure 2.3. The ice cores deeper than 50 m were drilled by electro-mechanical drills. The 2003 core was drilled by the Dokodemo-drill, a portable ice core drilling system developed by ILTS, Hokkaido University [Kohshima et al., 2002; Shiraiwa et al., 2004]. The 2004 core was drilled using the titanium electro-mechanical drill developed by GeoTech. Co., Ltd, Japan. Other shallower cores were drilled by hand augers manufactured by ILTS.

Table 2.1: *Ice cores drilled at the Summit Caldera of Mt Wrangell and the King Col, Mt. Logan*

Year	Depth [m]	Location (WGS84)	X-ray density sample depth [m]	Other measured properties	Reference
The Summit Caldera of Mt. Wrangell					
1982	44	62°00'13"N, 144°01'54"W	-	β-activity, δ ¹⁸ O	Benson [1984; personal commun.]
2003	50	61°59'54"N, 144°02'30"W	0.79-50.31	δD, Tritium	Shiraiwa et al. [2004], Yasunari et al. [2007]
2004	216	61°59'29"N, 144°02'15"W	1.54-40.37	-	-
2005 (2005a)	9	61°59'29"N, 144°02'15"W	-	δD	Matoba [personal commun.]
2005 (2005b)	17	61°59'29"N, 144°02'15"W	0.71-16.80	-	-
2006 (2006-1)	8	61°59'29"N, 144°02'15"W	0.80-8.33	δD	-
2006 (2006-2)	23	61°59'29"N, 144°02'15"W	3.54-22.92	-	-
2006 (2006-82)	14	62°00'13"N, 144°01'54"W	-	δD	-
The King Col, Mt. Logan					
2002	220	60°35'20"N, 144°36'15"W	1.30-70.39	δ ¹⁸ O, MSA, Tritium	Goto-Azuma [personal commun.]

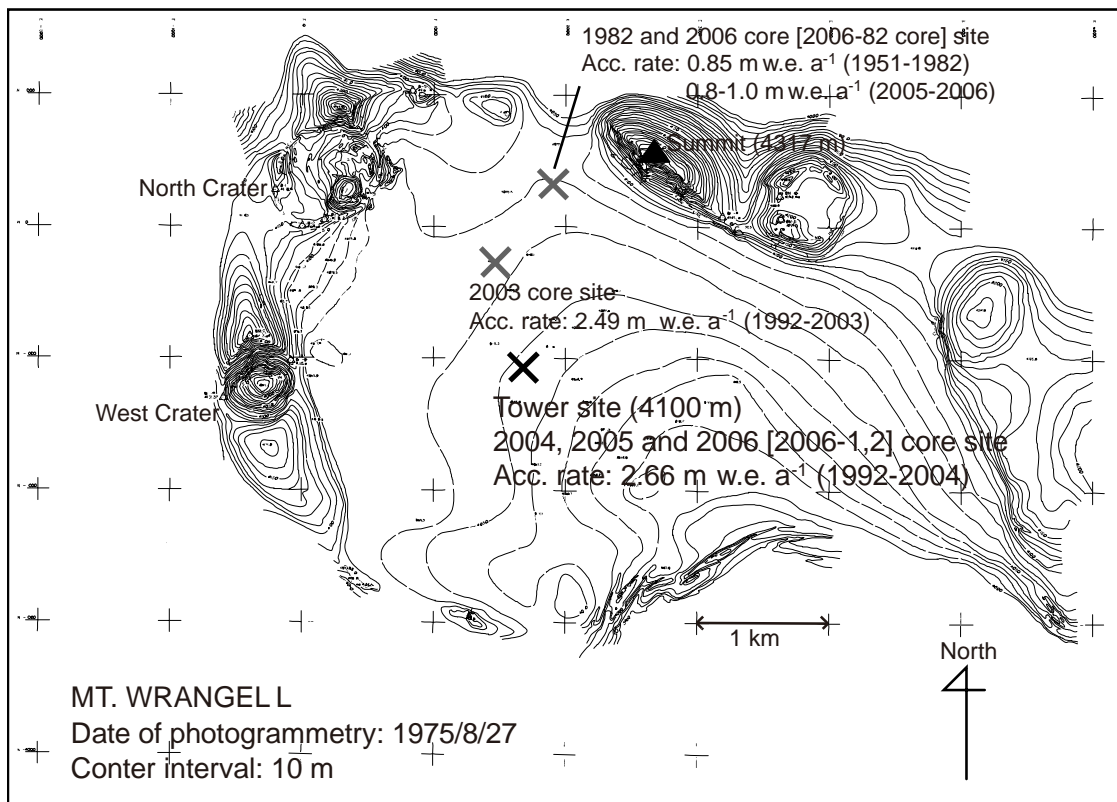


Figure 2.3: Topographic map of the Summit Caldera, Mt. Wrangell. Recent Ice core sites where ice cores were drilled in 2003-2006 and the 1982 core site by Benson [1984] are shown. Tower for the accumulation measurement was built at the same location with 2004-2006 core site. Averaged accumulation rate at each core site are shown with their locations. The original map was presented by Benson and Follett [1986].

2.1.3. King Col, Mt. Logan

King Col is snow-clad saddle between Mt. Logan (5959m) and King Peak (4137m). It is 0.5 x 0.5 km flat snow field and open for east-west direction [Fig. 2.4a and 2.4b]. The ice thickness is estimated to be 250 m by radio echo sounding [Kanamori, unpublished data]. An ice core was drilled to 220 m-deep using an electro-mechanical drill system developed by Takahashi [1996] in 2002 [Goto-Azuma et. al, 2003; Shiraiwa et al., 2003].

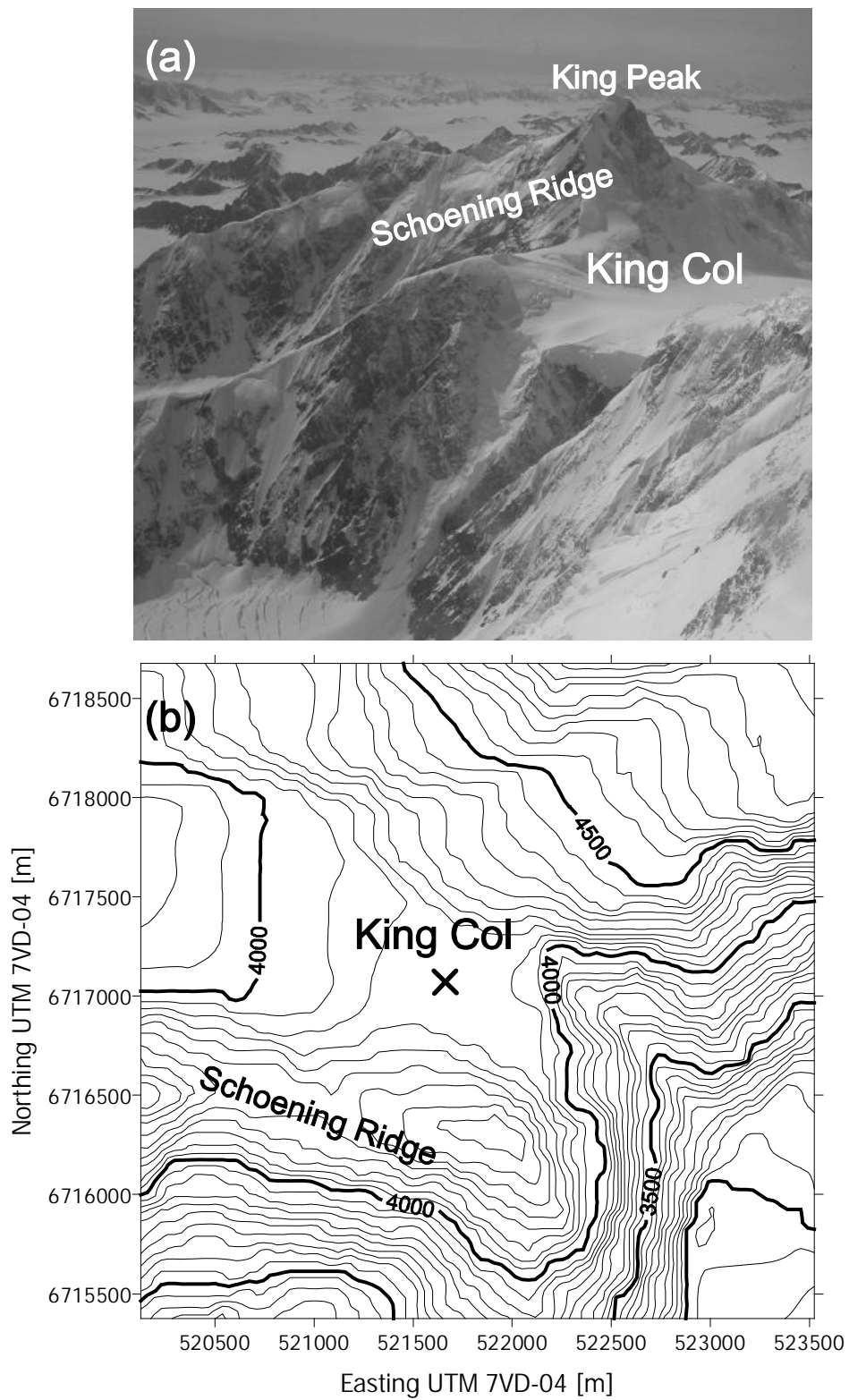


Figure 2.4: (a) Aerial photograph of the King Col (4135m) with the King Peak (5173m) from northeast side taken by Takayuki Shiraiwa in 2002. Schoening Ridge continue up to the King Peak from east side. (b) Topographic map of the King Col. “x” indicates the drilling site. Contour interval is 50m. The original map was presented by Shiraiwa [2003].

2.2. Spatial distribution of annual accumulation rate at the Summit Caldera, Mt. Wrangell

Spatial distribution of accumulation rate is important to examine spatial representation of the ice core information. Averaged annual accumulation rates for more than ten years are clearly known at three points in the Summit Caldera, Mt. Wrangell. The locations and the accumulation rates are shown in Fig. 2.3. The dating of a tephra layer from the 1992 Mt. Spurr eruption allowed a determination of averaged annual accumulation of 2.49 m w. e. (1992-2003) at the 2003 core site [Yasunari et al., 2007]. The same tephra layer was found at 52.6 m-depth in the 2004 core, which results in an averaged accumulation rate of 2.66 m w. e. (1992-2004) there. The 1982 core obtained by Benson was dated using the β -activity peak from nuclear tests in 1963. In addition, stable isotope profile shows annual periodicity and annual layer counting of stable isotope ratio gave dates before 1963 [Benson, unpublished data]; the averaged accumulation rate was 0.85 m w. e. (1951-1982). Another shallow surface core was obtained at proximity to 1982 core site in 2006. Hydrogen isotope ratio was analyzed using a mass spectrometer (JASCO International Co. Ltd., Isoprime PyrOH) every 0.05 m along core length for the ice core. The accumulation rate was then found to be 0.8-1.0 m w. e. (2005-2006) according to annual layer counting of the stable isotope ratio profile.

2.3. Accumulation measurements for individual storms on Mt. Wrangell

2.3.1. Method

To date individual accumulation events and examine characteristic features in density profile, which corresponds to snow surface condition, in situ accumulation

measurement was carried out at the Summit Caldera, Mt. Wrangell through a year. The location of measurements was set at the 2004 core site as shown in Figure 2.3. In June 2005 a metal tower was constructed and a total of 32 temperature sensors was installed on it so that snow accumulation could be measured by noting the time when snow burial suppressed the diurnal temperature cycle. The conventional method of using an acoustic sounder to measure the distance between the snow surface and the sensor above the surface was unsuitable at Mt. Wrangell because rime ice could disturb the sensor. A further problem is that rime ice and stormy weather at the summit might destroy the tower. Actually, heavy rime ice caused serious problem for meteorological instruments and snow survey poles in 1961 [Benson, 1968]. To reduce the risk of collapse, only a top five-meters of the tower was exposed above the snow surface in June 2005 (Fig. 2.5a). Although this was less than the expected annual accumulation of 6 to 7 m snow, it still covered most of the annual accumulation. An avalanche beacon (Ortovox, F-1 focus) was mounted at the middle of the tower with additional batteries to help us find the tower in the following year, in case of complete burial (Fig. 2.5a).

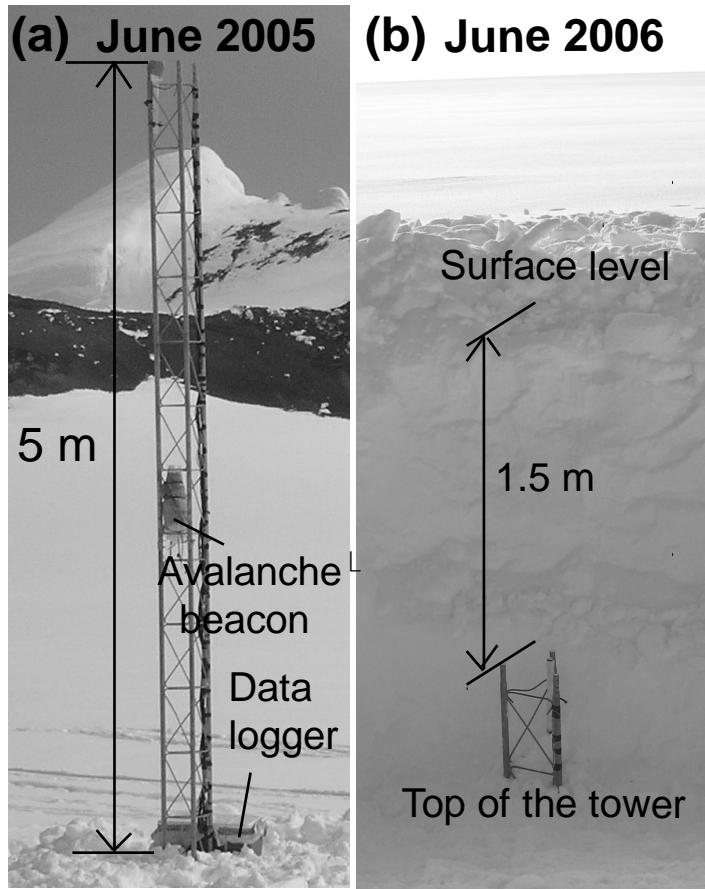


Figure 2.5: Pictures of the accumulation measurement tower at the Summit Caldera of Mt. Wrangell. (a) After installing the tower in June 2005. (b) After one year measurement in June 2006.

Thirty two sets of copper-constantan thermocouples were mounted on the tower at interval of 0.15 m, starting at 0.24 m above the June 3 snow surface. Hourly temperatures were recorded with a CR-10X (Campbell Scientific, Inc.) data logger and a multiplexer (AM16/32, Campbell Scientific, Inc.). An internal sensor of the data logger measured the reference temperature for the thermocouples. The data logger and multiplexer were kept in an insulated box. The accuracy of each temperature measurement is within $\pm 1.5^{\circ}\text{C}$. The temperature time series showed large variations in daily temperatures until they were buried by snow accumulation, which allowed the dates of burial to be determined. The detectable snow-height change by this method is

0.15 m and its time-resolution is one day, because the suppression of the daily temperature cycle can only be detected within about one day. The data was recovered in June 2006. At the time, the top of the tower was buried by 1.5 m of snow (Fig. 2.5b). To convert from snow depth to water-equivalent depth, a density profile was measured using a snow pit and ice cores to a depth of 8.3 m close to the tower's location in June 2006.

2.3.2. Results

Temperature data was obtained from 3 June 2005 to 22 June 2006. The thermocouples at 0.54, 2.79, 3.84 and 4.59 m above the initial snow surface had stopped working before their snow burials, but all others collected enough long records to determine the snow burial date. This temperature profiles were converted to snow height time series (Fig. 2.6; See Appendix A for temperature time series and the conversion). Total snow accumulation in the period was 6.48 m and the top of tower was buried by snow on 8 December 2005. Using the measured density profile, 6.48 m in snow was found to corresponded to 2.66 m w. e. The exact days of snow burial were determined for 70% of the total accumulation in water equivalent. In mid-August 2005, the snow height temporarily decreased. This was due to snow compaction caused by surface melting. At that time, thermocouples that had been buried recorded an increase of snow temperature to the melting point. In addition, ice lenses were found at the corresponding depth when the tower was dug out for data recovery, and in the ice core, there were a 10 mm thick granular snow layer and two 2 mm thick ice lenses. This was the only event in which any surface-lowering that exceeded the 0.15 m detection threshold was recorded.

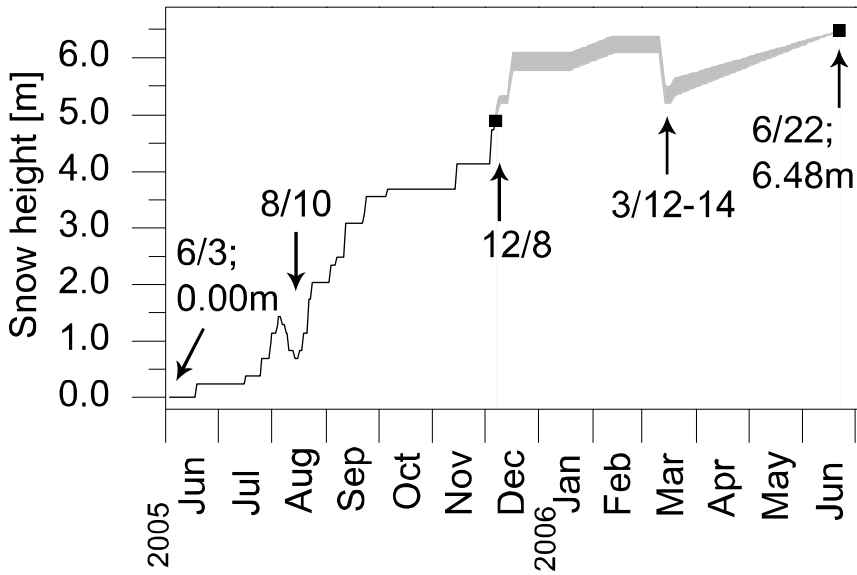


Figure 2.6: Snow height from 3 June 2005 to 22 June 2006 at the summit of Mt. Wrangell. The top of the tower became buried on 8 Dec 2005. The gray area shows range of estimated value between burial of the tower to the snow surface of 22 June 2006, which was 6.48 m above the snow surface of 3 June 2005.

Snow height time series after complete snow burial of the tower was estimated using the thermal diffusion equation

$$\frac{\partial T}{\partial t} = k \frac{\partial^2 T}{\partial z^2} \quad (2.1),$$

where T is temperature, t is time, k is thermal diffusivity and z is depth. The thermal diffusivity $k=K/\rho c$, where K is thermal conductivity, ρ is density and c is specific heat capacity. Thermal conductivity of snow was given by Devaux [1933], which gives empirical value for density range of 100-600 kgm⁻³. Vertical temperature profiles with 0.15 m interval were calculated by the thermal diffusion equation for the period after the tower burial. The initial temperature was given by measured value just before the snow burial. The time step was one hour. Surface temperature was given by estimated snow surface temperature calculated by a regression curve from Gulkana temperature data shown in Figure 4.1 (See chapter 4 for the temperature estimate). The 10m-deep

temperature was given -18.9°C , which is measured value in 2003 [Shiraiwa et al., 2004].

The calculated value by the model at each depth and measured value at the top of tower was compared (Fig. 2.7). The top of tower was estimated to be located at the depth range between two similar wave forms. Possible range of snow height was shown in Figure 2.6. There was a surface lowering event on mid March which appeared as fluctuation in relative short time of measured temperature profile.

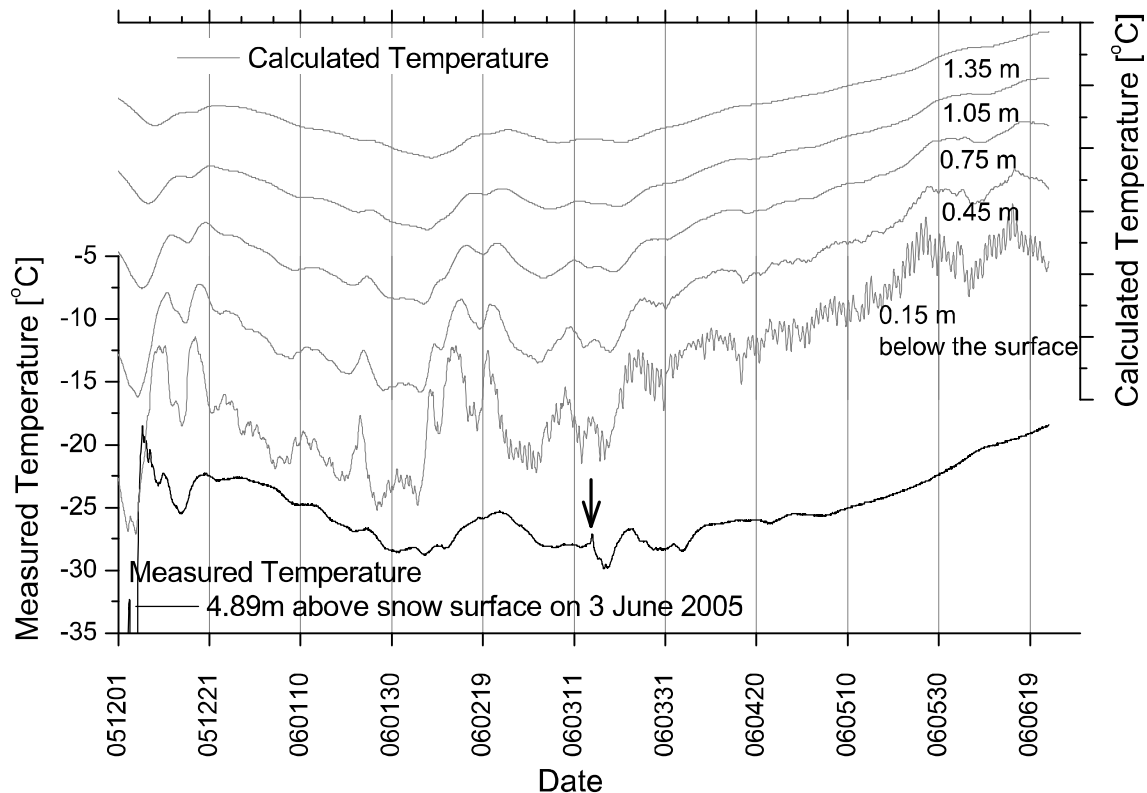


Figure 2.7: Comparison of measured temperature at the top of accumulation measurement tower after snow burial on December 2005 and calculated temperatures which expects snow temperature at certain depths. The top of tower is expected to be located at the depth temperature of that shows most similar fluctuations. The scale of calculated temperatures are same with the scale of measured temperature but vertically lagged for comparison in the figure. The arrow indicates timing of erosion event which is assumed from sharp fluctuation in the measured temperature profile.

2.4. Density measurements

2.4.1. Method

Setting of the measurement system

Detailed density profiles were measured by the X-ray transmission method [Hori et al., 1999]. In this method, intensity of transmitted X-ray through an ice core sample is converted to the density value of the ice core sample using a calibration curve which describe transmitted X-ray intensities as a function of thickness of pure bulk ice.

Figure 2.8 shows a schematic picture of the measurement system which is operated at -20 °C. A thick ice core sample on the sample stage moves through the X-ray beam perpendicularly with constant velocity and the transmitted X-ray is measured by a scintillation counter continuously. The value was averaged every 1mm along core length. The X-ray generator was operated at 30 kV. The width of optical slit was limited to 0.05 mm for a divergence slit, 0.2 mm for a scattering slit and 0.2 mm for a receiving slit. The height of the scattering slit was 20 mm.

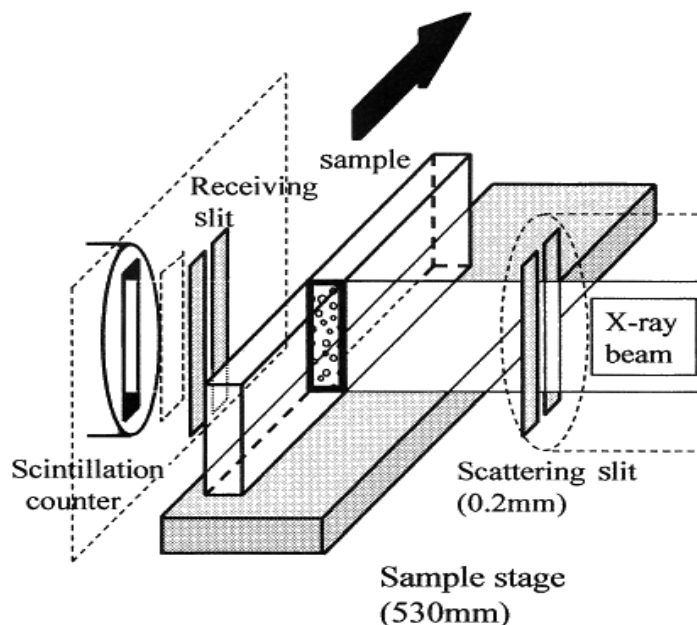


Figure 2.8: A schematic picture of the X-ray transmission measurement system (Hori et al., 1999; Partly modified).

Ice core samples

Detailed density was measured for the Mt. Wrangell ice cores drilled in 2003, 2004, 2005, 2006 and the King Col ice core drilled in 2002. The measured ice cores and their lengths are shown in Table 2.1. Figure 2.9 shows cross sections of each ice core. The thick sections of ice core samples were cut by bandsawing then planed by microtome. The samples were typically about 500 mm long and 35 mm thick. Thickness of each sample was measured by a vernier caliper with an accuracy of 0.1 mm for density calculations.

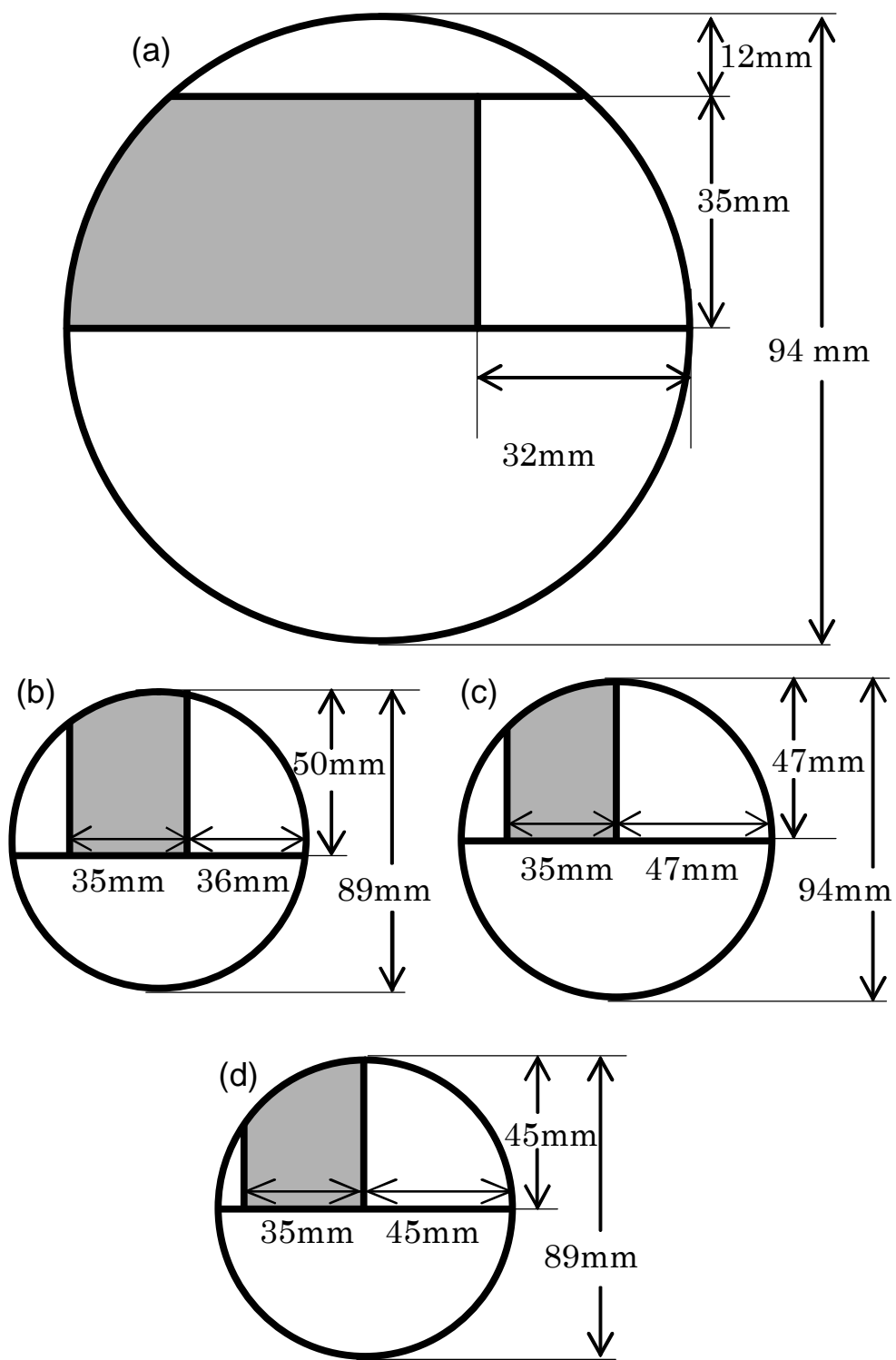


Figure 2.9: Cross sections of the ice core samples. Lines in each circle corresponding to cutting line by a band saw. Gray areas were used detailed density measurement. Scale is 1:1 for Fig. 2.9a and 1:2 for other three pictures. (a)King Col core. (b)Mt. Wrangell 2003 core. (c)Mt. Wrangell 2004 core. (d)Mt. Wrangell 2005, 2006-1 and 2006-2 core.

Data conversion and calibration

The density ρ is calculated as

$$\rho = \rho_{ice} \frac{t_{eff}}{t_s} \quad (2.2)$$

where ρ_{ice} is density of pure bulk ice, 918.3 at -20°C and t_s is thickness of the core sample. The value of t_{eff} is assumed from transmitted X-ray intensities using a calibration curve.

Because continuous X-ray is used for the measurement, wavelength dependence of X-ray absorption have to be taken into account in the calibration. The measured fraction transmitted, f is described as;

$$f = \frac{\int_{\lambda_{min}}^{\infty} I_0(\lambda) \exp(-\mu(\lambda)t_{eff}) d\lambda}{\int_{\lambda_{min}}^{\infty} I_0(\lambda) d\lambda} \quad (2.3).$$

Here, $I_0(\lambda)$ is intensity of incident X-ray, which is function of wavelength λ . The minimum λ in the spectrum is λ_{min} . $\mu(\lambda)$ is the linear absorption coefficient of pure ice, which is dependent of λ . t_{eff} is effective thickness of the sample. Because f cannot be calculated theoretically, the relation between t_{eff} and f is assumed using a calibration curve,

$$f = A_1 \exp(-B_1 t_{eff}) + A_2 \exp(-B_2 t_{eff}) + y_0 \quad (2.3).$$

Here, A_1 , A_2 , B_1 , B_2 and y_0 are fitting parameters. Although f should be expressed by infinite number of the exponential terms theoretically, only two exponential terms were calculated to avoid over fitting for limited number of data samples.

Figure 2.10 shows the calibration curve. Samples for the calibration were obtained from clear, no visible air bubble part of ice thickness of which was considered

as t_{eff} . The fitting parameters are also shown in Fig. 2.10. The R^2 value of the calibration was 0.99924 and χ^2/df was 0.00004, hence f was almost described as induced variable of t_{eff} and error in the fitting is relatively small than other errors described in the next subsection.

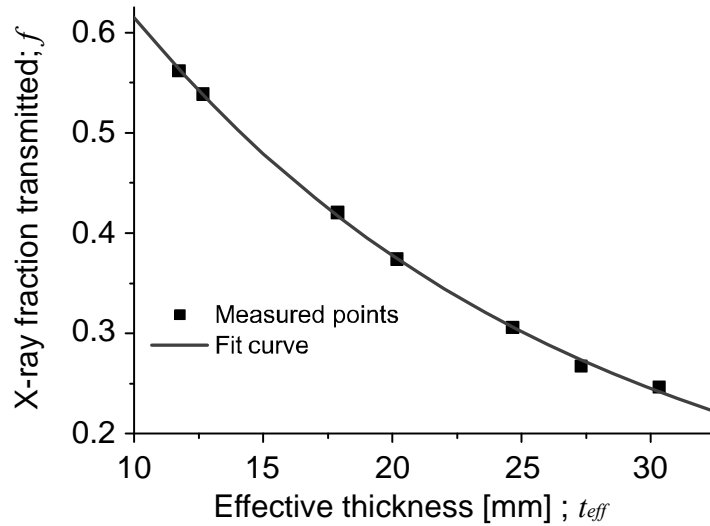


Figure 2.10: Calibration curve for the density calculation. The equation and fitting parameters are;

$$f = A_1 \exp\left(\frac{-t_{eff}}{B_1}\right) + A_2 \exp\left(\frac{-t_{eff}}{B_2}\right) + y_0$$

$A_1: 0.4813$	$A_2: 0.4813$
$B_1: 17.18895$	$B_2: 17.18895$
$y_0: 0.07694$	

$$\chi^2/\text{DoF} = 0.00004 \text{ and } R^2 = 0.99924.$$

Errors

Principally, the following two errors are considered;

1. errors associated with the sample thickness measurement by a vernier caliper,
2. statistical variations of X-ray intensity.

Error 1 is within 1% of the thickness. Thickness of the sample was about 35 mm and the accuracy of the measurement was within 0.1 mm. Error 2 is within 0.5% of X-ray

intensity. Statistical variations of X-ray are known to be $1/N^{0.5}$ (N : intensities of X-ray) empirically, and N at the measurement was more than 6×10^4 counts. Therefore the total error is considered to be within 1%.

2.4.2. Results and discussion

Figure 2.11 shows X-ray density profiles and conventional volumetric density profiles at the Summit Caldera of Mt. Wrangell and King Col. The X-ray density profiles overlaps volumetric density profiles well. Although density seems monotonically increased with depth in the volumetric density profiles, it is fluctuated in the high resolution profiles by the X-ray transmission method. Most of positive spikes in the profiles correspond to melt features which appeared as ice lenses in visual stratigraphy. The higher densities in the King Col profile, in contrast to those of Mt. Wrangell's at same depths seems to be caused by higher initial density and lower accumulation rate, which keeps time passed denser firn in shallower part at King Col.

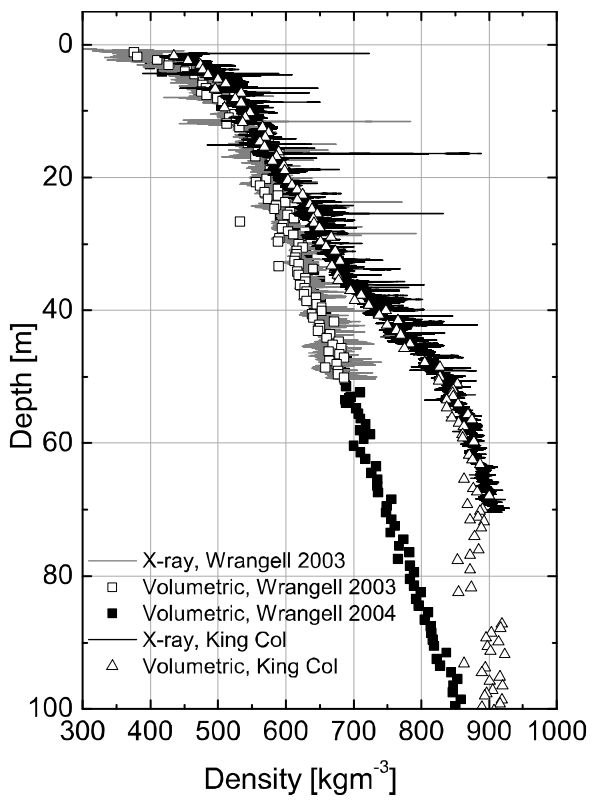


Figure 2.11: Density profiles by X-ray transmission method and volumetric method at the Summit Caldera of Mt. Wrangell and the King Col, Mt. Logan.

Density range of 820-840 kgm^{-3} , which corresponds to close-off depth, appeared at about 90m-deep at Mt. Wrangell profiles. Such a deep close-off depth had appeared only in inland of ice sheets [Paterson, 1994], where 10m depth temperatures are less than -50°C . Hence, Mt. Wrangell is a unique case. Probably, this is because of high accumulation rate which is about $2.5 \text{ m w. e. a}^{-1}$ at the Summit Caldera of Mt. Wrangell. The value is about 10^3 times higher than inland of ice sheets. Close-off depth is determined by combination of initial density, accumulation rate and densification rate. At Mt. Wrangell, effect of accumulation rate seems to be large; i.e. a surface layer goes deep by highly accumulated snow in short period. The ice age at the close-off depth is estimated to be 30 years. This is much younger than the value of the inland of ice sheets which is more than 1k years old.

The King Col profile is also unique because of its bending at the profile. The slope of depth-density curve increased at depth of about 40 m. This is unusual and never appears under steady state condition. Another point to be mentioned in the King Col profile is fluctuations appeared in the density range over 900 kgm^{-3} . The fluctuation of density is still detectable in the density range. Error range in the relative density value is within 0.5% because it depends on error in statistical variations of X-ray intensity. Hence, some of the fluctuations in the density range over 900 kgm^{-3} are significant.

Figure 2.12 shows density profiles at the Summit Caldera of Mt. Wrangell for four years. All ice cores were drilled at almost same place except the 2003 core which is 700 m NNW from the other sites. The four profiles are overlapped. It means that the profiles agree with Sorge's law [Bader, 1954] which states depth-density profile is invariant with time under conditions of constant accumulation rate and time. However, fluctuations in the density profiles doesn't overlap. This means detailed density profiles reflects variations of accumulation rate and temperatures in short periods such as monthly to daily time scale. Fluctuations with millimeter scale wavelength seems to correspond to daily scale changes in surface conditions.

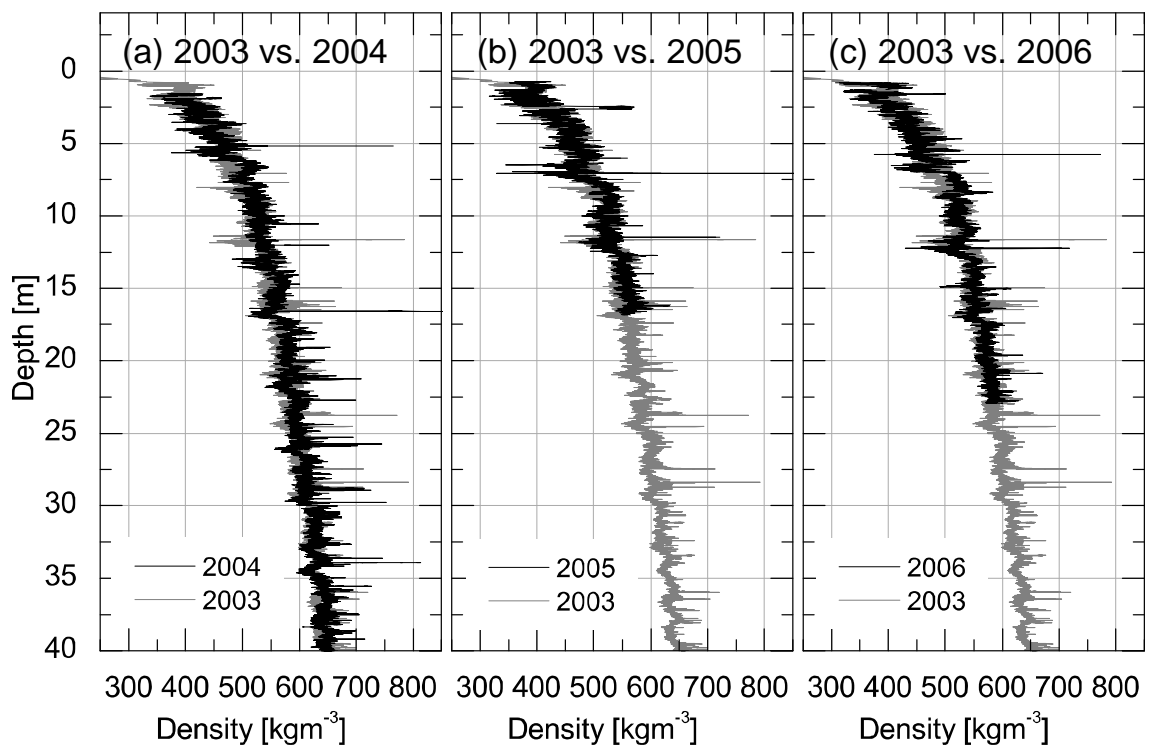


Figure 2.12: Detailed density profiles at the Summit Caldera of Mt. Wrangell. (a) density profiles of the 2003 core and the 2004 core. (b) density profiles of the 2003 core and the 2005(2005b) core. (c) density profiles of the 2003 core and the 2006(2006-1,2) core.

3. Interpretation of detailed density profiles at Mt. Wrangell

3.1. Relationship between surface condition and density profile

In order to connect characteristics in density profile and surface conditions, detailed density profile and visual stratigraphy of the Mt. Wrangell 2006 core were compared with the measured accumulation time series and temperature profiles. Temperature profiles of snow cover and accumulation time series estimated by the temperature profile were recorded from 3 June 2005 to 22 June 2006. Daily accumulation data were extracted until 7 December 2005 when top of the measurement tower was varied by snow. Exact date of each depth is not directly recorded in the core because accumulation rate at each event in water equivalent is unknown. Therefore the date is assumed from the comparison. In the ice core, dates of two depths was identified clearly. One is 3 June 2005 which the measurement tower was built on and the other is 10 August 2005 when the melt event occurred on. The surface level on 3 June is obviously determined by the tower basement. Melt features in an ice core is formed after some percolation [Benson, 1962]. In the case of the 2006 core, granular snow layer appeared just above the clear ice lenses in visual stratigraphy. Therefore the granular snow layer was considered as the surface level of the melt event. In addition, surface level of the tower burial day was estimated from water equivalent depth. According to Sorge's law, depth-density curve is invariant with time. At the time of tower burial, snow height from the bottom of tower height was 4.89 m and it correspond to 1.92 m w. e. at the site. Therefore 1.92 m w. e. above the tower basement depth in the ice core was estimated to be surface level at the tower burial. These three points were controls on the dating of the 2006 core.

Figure 3.1 shows integrated value of the measured daily accumulation and the

ice core data. Boundaries of measured accumulation events in the integrated accumulation data indicate position of approximate corresponding boundaries in the ice core depth. If density of newly accumulated snow were constant, this approximation would become accurate. The corresponding depths to the accumulation event boundaries were estimated from the approximate position by the measured accumulation data and visual stratigraphy of the ice core (Fig. 3.1; See Appendix B for detail of the visual stratigraphy). The stratigraphic features that were estimated to be correspond to accumulation event boundaries were shown in table 3.1. It seems that estimated boundaries of accumulation events by individual storms appears as stepwise changes in detailed density profiles. The author assume that boundaries of accumulation events appear as stepwise change in density profile because such density differences is the most possibly formed at storm event boundaries as following conditions. Just before snow accumulation event, snow surface tend to be denser because of sintering, wind packing or a surface crust layer. Density of new snow is relatively low; therefore such structure with stepwise change of density can be formed. Another possible cause of stepwise change in a density profile is wind erosion. When wind erosion occurs, softer surface snow is most likely eroded and denser layer can remain at the surface. In addition, thick denser layer can be formed by wind compaction. Actually, rectangular shape of density profile (Fig. 3.1) is assumed to be formed by erosion event, which occurred in mid March (Fig. 2.6). This pattern is also included in boundaries of accumulation events.

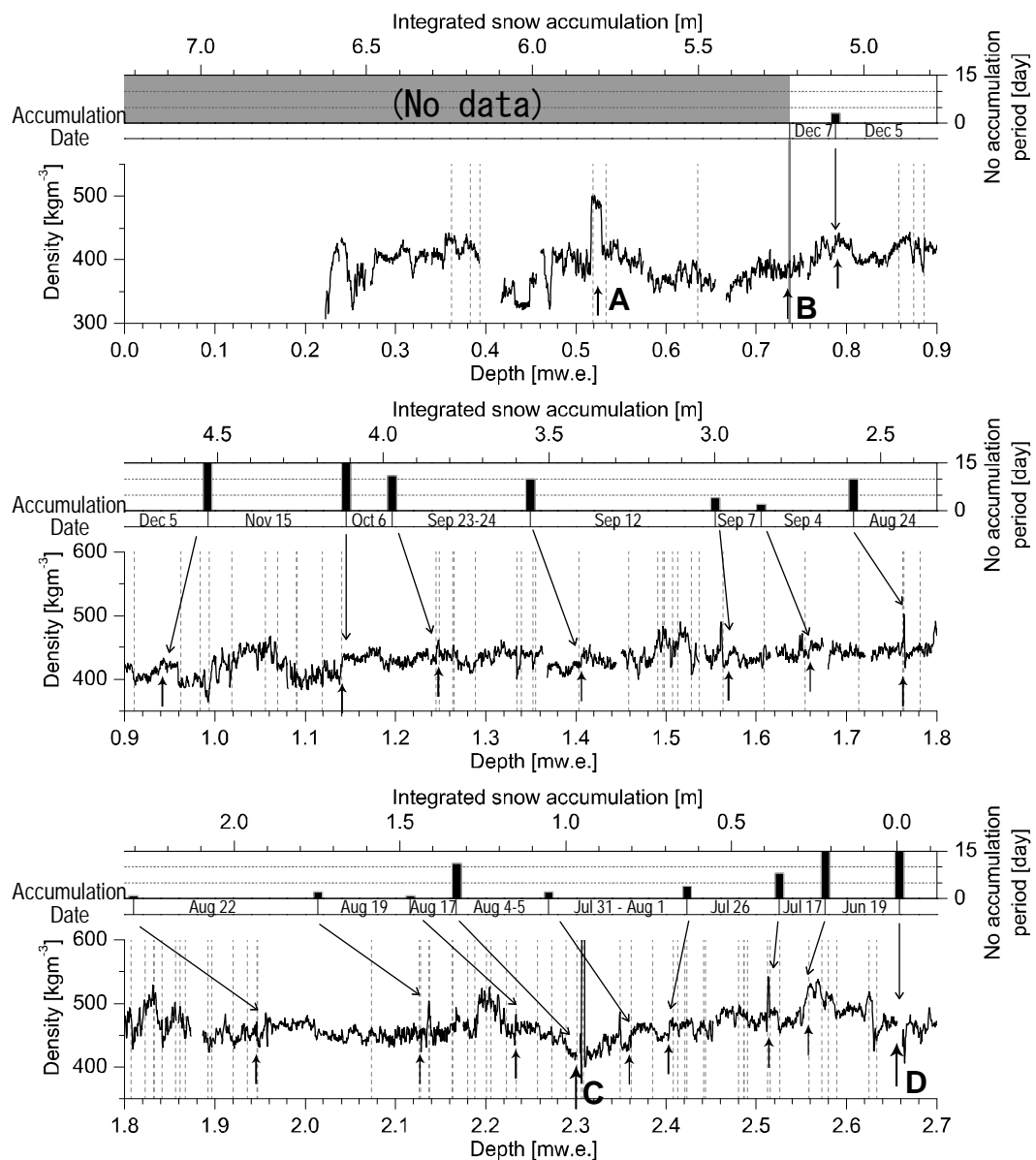


Figure 3.1: Comparison of integrated value of measured snow accumulation and ice core data. Upper chart: Integrated value of snow accumulation from 3 June to 8 December in 2005 (blocks with date) and no accumulation period between accumulation events (vertical bars). Lower chart: Detailed density profile (black solid line) and layer boundaries in visual stratigraphy (vertical break lines) of the Mt. Wrangell 2006-1 core. A: Characteristic density profile which is assumed to be correspond to an erosion event in mid March. B: Estimated surface depth at the tower burial on December 8 2005. C: Depth of surface melt event on August 10-13. D: Depth of snow surface on June 3 2005. Scale of the upper chart and lower chart are fitted at the point of June 3 and December 8. Corresponding points in both charts are indicated by arrows.

Table 3.1: Dated depths on the Mt. Wrangell 2006-1 core

Date	Depth [m]	Depth [m w.e.]	Type	Descriptions	Supposed condition
2005/6/3	6.48	2.66	Control	Depth of the tower base	Surface at the field work in 2005
2005/6/19-7/17	6.26	2.55	Storm event boundary	Dense layer with fine grains; texture is different from layer above	Wind packed layer; exposed to the surface for a while
2005/7/17-7/26	6.18	2.51	Storm event boundary	Dense layer including large grain; may be melt feature	Melt layer by solar radiation or high temperature; Exposed to the surface for a while
2005/7/26-31	5.94	2.40	Storm event boundary	Dense layer with fine grains; texture is different from layer above	Wind packed layer; exposed to the surface for a while
2005/8/1-4	5.86	2.36	Storm event boundary	Texture is coarser at the layer above; stepwise change in density	Exposed to the surface for a while
2005/8/5-17	5.72	2.30	Melt feature	Granular snow just above a clear ice lens	Surface layer at melt events
2005/8/17-19	5.54	2.23	Storm event boundary	Boundary of coarse grain layers (above) and a fine grain layer (below)	Boundary of individual storms
2005/8/19-22	5.36	2.14	Storm event boundary	Top side of various texture layers Bottom side of a thick layer with small density variation	Boundary of individual storms
2005/8/22-24	4.95	1.95	Storm event boundary	Top side of a thick layer with small density variation; Bottom side of various texture layers	Boundary of individual storms
2005/8/24-9/4	4.54	1.76	Storm event boundary	Thin coarse grain layer; Top of various texture layers	Boundary of individual storms
2005/9/4-7	4.31	1.66	Storm event boundary	Stepwise change in the density profile	Boundary of individual storms
2005/9/7-12	4.10	1.57	Storm event boundary	Stepwise change in the density profile; Bottom of various texture layers	Boundary of individual storms
2005/9/12-23	3.73	1.41	Storm event boundary	Stepwise change in the density profile; layer boundary in visual stratigraphy	Boundary of individual storms
2005/9/24-10/6	3.36	1.25	Storm event boundary	Dense layer with fine grains; Top of layers with fine grains	Wind packed layer; exposed to the surface under windy condition for a while
2005/10/6-11/15	3.12	1.14	Storm event boundary	Clear stepwise change in the density profile; top of a thick layer with fine grains	Wind packed layer; exposed to the surface under windy condition for a while
2005/11/15-12/5	2.63	0.94	Storm event boundary	Stepwise change in the density profile	Boundary of individual storms
2005/12/5-7	2.27	0.79	Storm event boundary	Higher density structure at the expected depths range of the event boundary	Boundary of individual storms
2005/12/7	2.14	0.74	Estimate	Estimated depth of the surface at the tower burial	-
2006/3/12-14	1.57	0.52	Erosion event	Rectangle shape of the density profile; fine grains	Erosion event which was assumed from temperature profile
2006/6/22	0.00	0.00	Control	Surface level at the ice coring	-

Another kind of density peaks which is broader positive peak consists of several small peaks appeared in the detailed density profile. One can see such features in accumulation event on August 19, August 24, September 12 and November 15 (Fig. 3.1). These were nonuniform snow layers in visual stratigraphy associated with larger density variations. The small density peaks correspond to snow layers which consists of round large grains (diameter: 1-2 mm) and smaller particles (See appendix B for detail). These series of small peaks were supposed to be formed in an individual storm event according to the result of dating. Figure 3.2 shows temperature profiles at the accumulation measurement tower in the storm events in August and September 2006. Some high temperatures above 0°C is probably caused by solar radiation. When accumulation events which formed the large density variation layers had occurred, surface snow temperature had been above -10°C approximately. At the accumulation event which formed snow layers with low density variations in August 17, 22, September 4 and September 7, surface snow temperature had been about below -10°C approximately. It seems that relatively warm storm events form density peaks with large variations in the accumulated snow. This correspondence between the characteristic density layers and warm storm events support validity of the dating.

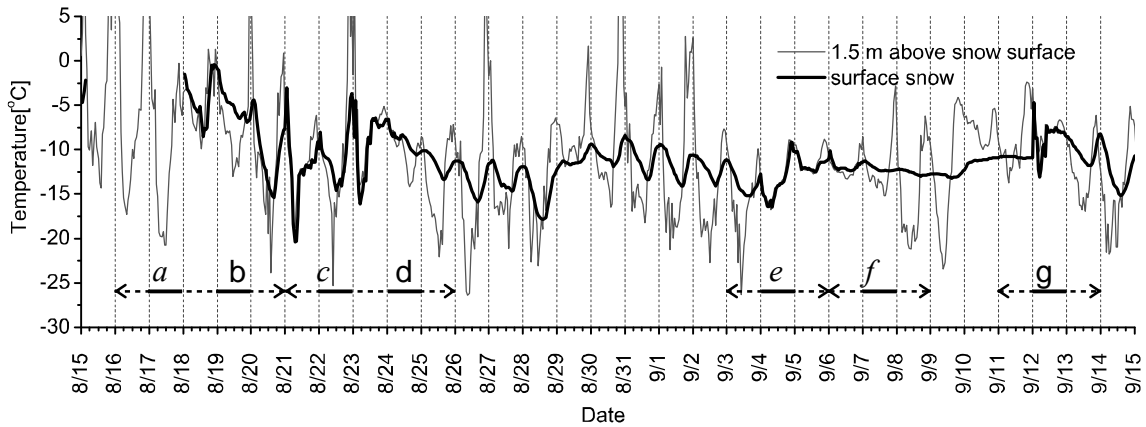


Figure 3.2: Temperature profiles at 1.5 m above snow surface (gray line) and surface snow temperature (0-0.15 m below the surface; thinner black line) during summer accumulation season in 2005 measured without shades. Arrows indicate periods of accumulation events (solid line) with error ranges (break line). Arrow b, d and g: accumulation event with large density variations; arrow a, c, e and f: accumulation event with small density variations (Fig. 3.1).

3.2. Effect of densification on detailed density profiles

Correspondence of stepwise changes in density profile and accumulation event boundaries were confirmed in snow layers accumulated in a year, density range of which was about $370\text{-}470 \text{ kgm}^{-3}$. This range is the first stage of densification dominant process of which is characterized by mechanical packing of snow [Maeno and Kuroda, 1986]. Density is the most variable in densification process at the range. Li and Zwally [2002] explained that annual fluctuation of density profile is induced in densification process after snow deposition at the summit of Greenland from model result. This variation of density occurred in the first stage of densification process. Gerland et al. [1999] reported that higher density in winter layers and lower density in summer layers at shallower part were reversed at deeper part in the ice core drilled at Barkner Island, Antarctica. To extend the discussion to deeper part, it needs to examine whether the stepwise feature of density profile is preserved over years in densification process or

not.

Figure 3.3 shows density profiles of the ice cores drilled at the Summit Caldera of Mt. Wrangell from 2003 to 2006. Shape of density profiles are similar and stepwise features in density profiles are preserved in the first stage of densification process density range of which is to 550 kgm^{-3} . Although the 2003 core was drilled 700 m away from the site of other cores, characteristic features in the density profiles were consistent. Figure 3.4 shows density profiles of the Mt. Wrangell 2003 and 2004 cores at greater depth. Shapes of the two profiles are very similar at $550\text{-}700 \text{ kgm}^{-3}$ range like the case of shallow parts. Therefore stepwise changes in density profiles are also kept at this density range. Hence, stepwise changes in density profile is considered to reflect past storm event boundaries not only in surface snow layers but also in deep firn layers.

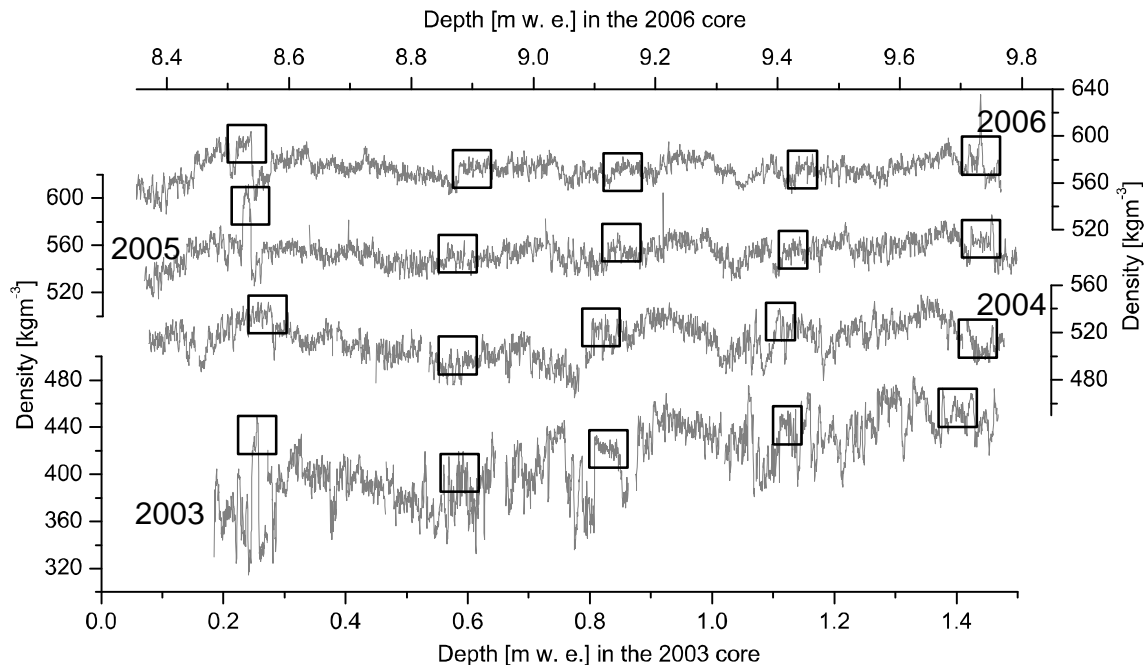


Figure 3.3: Temporally corresponding part of density profiles of Mt. Wrangell ice cores drilled in 2003, 2004, 2005 and 2006. Vertical series of boxes indicates examples of stepwise changes that were kept for three years through densification process.

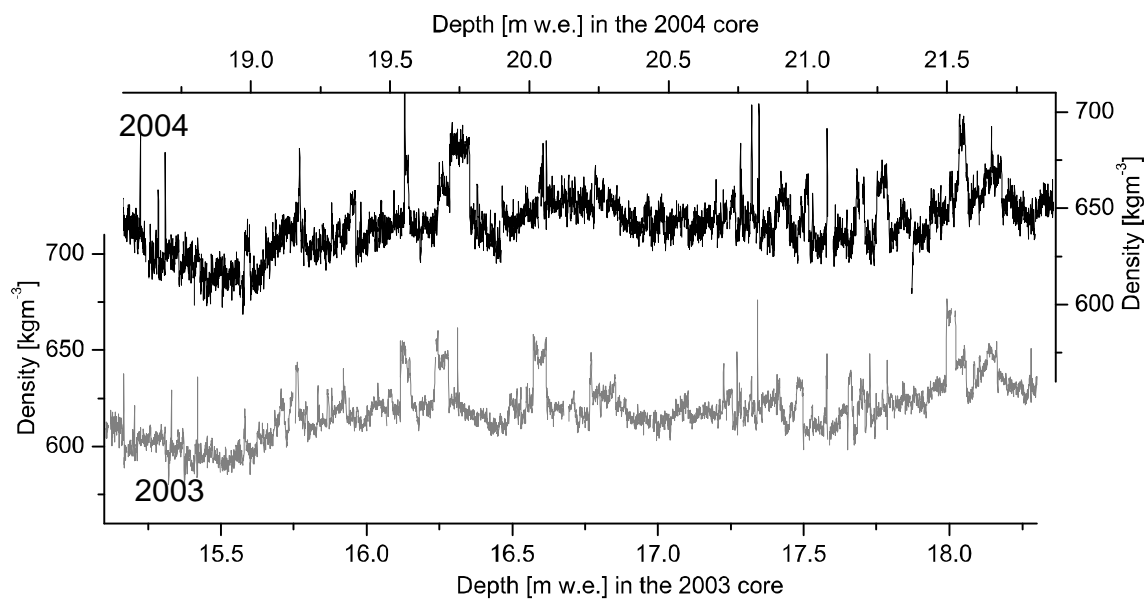


Figure 3.4: Temporally corresponding part of density profiles of the Mt. Wrangell 2003 core (gray line) and 2004 core (black line).

4. Detailed dating of Mt. Wrangell cores

4.1. Estimation of surface condition at Mt. Wrangell from weather station data

The Mt. Wrangell 2006 core was well dated by the in situ snow accumulation measurement. However, the measurement period was limited only one year. To date the older ice cores, we need such information for the past. Fortunately, precipitation and temperature data are available from the early 20th century at national weather observatories around Mt. Wrangell. To estimate the surface condition for the past, relationship between surface condition at the ice coring site on Mt. Wrangell and the weather station's data around Mt. Wrangell were examined for following three topics; 1)snow temperature at Mt. Wrangell was compared with temperature at the weather stations to estimate timing of melt events; 2)seasonal snow accumulation pattern at Mt. Wrangell was compared with seasonal precipitation pattern at the weather stations to estimate seasonal accumulation pattern for the past; 3)timing and amount of individual accumulation events at Mt. Wrangell were compared with those of precipitation events at the weather stations to date individual accumulation event found in the ice core.

Data from four weather stations; Gulkana, Yakutat, Valdez and Cordova were used for the comparison. These weather station data are from the U.S. National Weather Service. The four stations that were selected are the closest weather stations to Mt. Wrangell in south central Alaska (Fig. 2.1). Table 4.1 shows their locations, elevations, mean annual precipitation and mean annual temperature. Gulkana has much less precipitation than the three coastal stations because it is located in the precipitation shadow of the coastal mountains and the Wrangell-St.Elias Mountains.

Table 4.1: Primary information of four weather stations in south central Alaska

Weather station	Location	Elevation [m]	Mean annual precipitation* [mm]	Mean annual temperature* [°C]
Gulkana	62°09'N, 145°27'W	481	290	-2.7
Yakutat	59°31'N, 139°40'W	9	4074	4.2
Valdez	61°08'N, 146°21'W	10	1712	3.5
Cordova	60°30'N, 145°30'W	13	2445	3.9

*NCDC 30 year normal (1971-2000); Alaska Climate Summaries,

<http://www.wrcc.dri.edu/summary/climsmak.html>

Figure 4.1 shows scatter diagram of hourly surface snow temperature at Mt. Wrangell and hourly air temperature at Gulkana. The surface snow temperature was measured by sensors which is the closest to the surface in snow buried sensors at the time. Its depth should be 0-0.15 m from the surface. The period of data is from 19 June to 8 December in 2005. The surface snow temperature is highly correlated with Gulkana temperature ($R=0.86$) and this is the best correlation in the four stations. The author suppose that the best correlation at Cordova in the four stations are because of the closest location. This correlation made it possible to estimate snow surface temperature and timing of melt event at Mt. Wrangell from the lowland temperature. Melt features appeared a few times in each annual layer of the ice core. These melt features were most likely formed at the timing when the highest temperatures were recorded. The relationship between temperatures at Mt. Wrangell and Gulkana was already pointed out by Benson [1968]. Benson stated that warm sunny weather which affect both top of Mt. Wrangell and Gulkana are the best time for potential melting and found excellent index for such a weather, i. e. the warm sunny weathers come when air temperature exceed 25°C at Gulkana. The correlation shown in Figure 4.1 agreed with Benson's index.

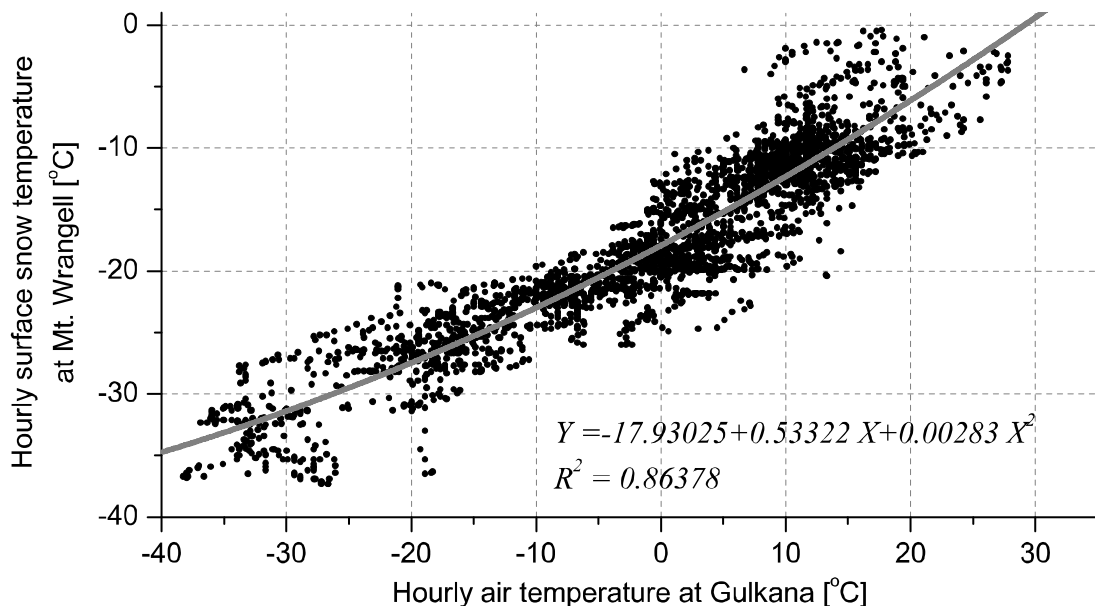


Figure 4.1: Scatter diagram of hourly air temperature at Gulkana and hourly surface snow temperature at Mt. Wrangell in 2005 with regression curve by quadratic polynomial fitting.

Figure 4.2 shows cumulative accumulation at Mt. Wrangell and cumulative precipitation at the four weather stations. At Mt. Wrangell, 50% of the annual accumulation was observed in two months from the end of July to the end of September. Weather station data at Cordova show a similar cumulative precipitation pattern. Despite the closer location of Gulkana, the fraction of the annual precipitation received from June to early August is much higher than at Mt. Wrangell. Valdez and Yakutat data show a more gradual seasonal increase than Cordova. Both places had lower relative fall precipitation and higher relative winter precipitation than Cordova and Mt. Wrangell. The 2005-2006 year seems to have a normal seasonal precipitation distribution at Cordova. Figure 4.3 shows the net 30 year-average of the monthly precipitation fraction from June 1972 to May 2005 in Cordova and the fraction from June 2005 to May 2006. Although monthly fractions were different from January to May, higher precipitation from late summer to fall (August to October) is common. It is therefore reasonable to

assume that the normal precipitation pattern at Mt. Wrangell also follows this pattern.

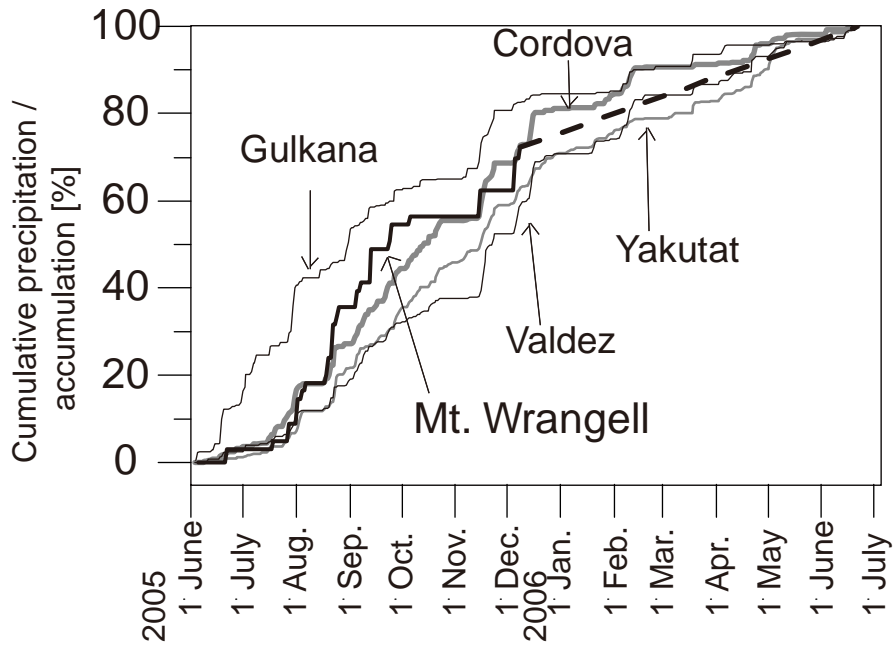


Figure 4.2: Cumulative accumulation at Mt. Wrangell (thick black line) and cumulative precipitation at four weather stations (Gulkana: thin black line; Yakutat: thin gray line; Valdez: thin black line; Cordova: thick gray line) in south central Alaska, from 3 June 2005 to 22 June 2006. The values are expressed as percentage of the total amount during the time period.

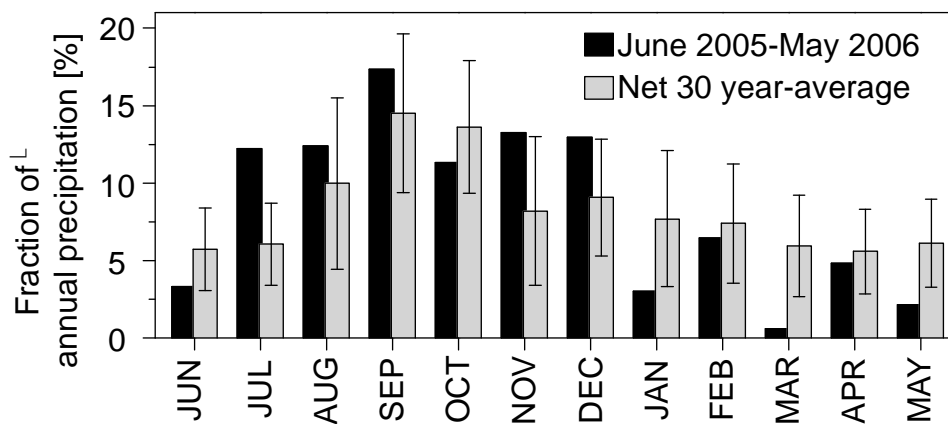


Figure 4.3: Comparison of monthly precipitation in the observation year (June 2005 to May 2006) with the 30-year average at Cordova. The error bars show standard deviations. The monthly values are expressed as percentages of the annual precipitation for each year. The net 30-year average is calculated with the data from June 1972 to May 2005. The data of 1985, 1990 and 1999 were excluded because there are some missing values in the original precipitation record.

Figure 4.4 shows daily accumulation at Mt. Wrangell that exceeded the detection threshold and daily precipitation at the four weather stations. When Mt. Wrangell had detectable snow accumulation events, the weather stations also show precipitation events. This correspondence is particularly clear for Cordova and Valdez. These two coastal weather stations seem to be located at path of storms that bring accumulation to Mt. Wrangell. To evaluate more quantitatively, precipitation events at Cordova and accumulation events at Mt. Wrangell were compared. Each continuous precipitation or accumulation event was regarded as one storm event. Some events which occurred with one day interval between them at Mt. Wrangell were counted as single events for comparison because corresponding events at Cordova were continuous ones. From June 3 to December 8 in 2005, there were 34 storm events at Cordova and 14 of them occurred simultaneously with storm events at Mt. Wrangell (Fig. 4.4). Figure 4.5 shows a histogram of precipitation events at Cordova. Most of the storm events with less than 20 mm precipitation had no corresponding accumulation event large enough to exceed the detection threshold on Mt. Wrangell. On the other hand, all of the storm events with more than 70 mm precipitation were associated with recorded storm events on Mt. Wrangell. From these results, it is reasonable to consider that Mt. Wrangell has no storm events when Cordova has no precipitation or storm events precipitation of which is less than 20 mm. Figure 4.6 shows a scatter plot of precipitation at Cordova and accumulation at Mt. Wrangell for each corresponding storm event. The data show a positive dependency, but poor linear correlation ($R=0.29$); it is therefore difficult to estimate the amount of accumulation by individual storms on Mt. Wrangell from Cordova precipitation.

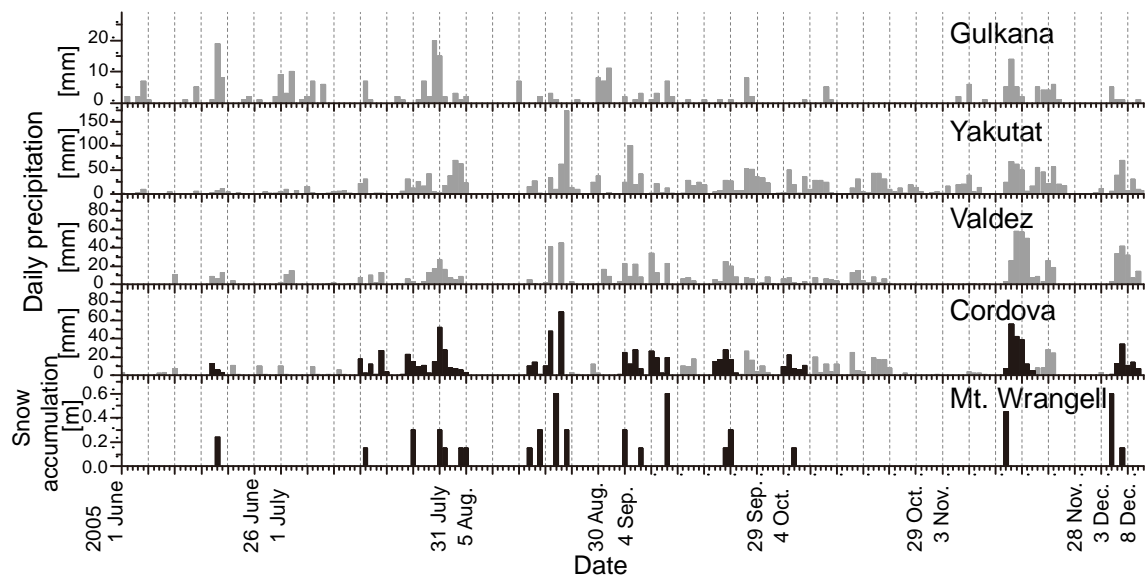


Figure 4.4: Daily snow accumulation rate at Mt. Wrangell and daily precipitation rate at four weather stations in south central Alaska. Daily data at Mt. Wrangell is unknown after 8 December. The coincident events on Mt. Wrangell and Cordova are shown as black bars.

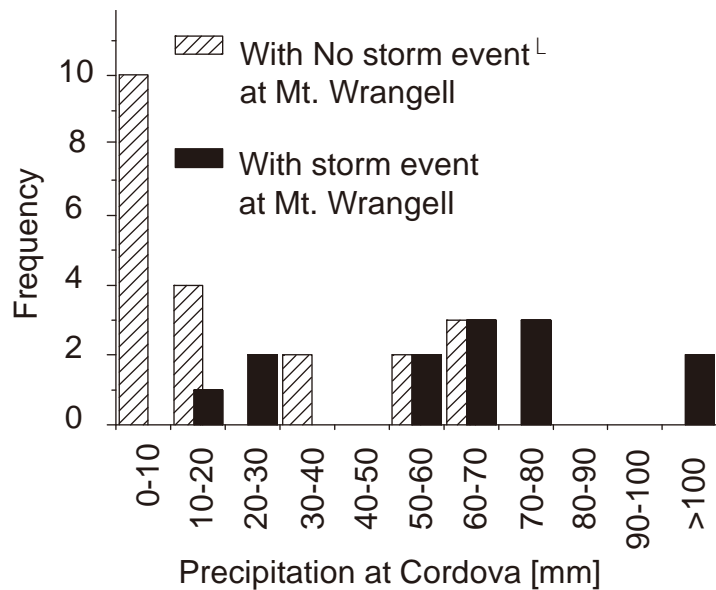


Figure 4.5: Histograms of Cordova storm events from June 3 2005 to December 8 2005. The hatched bars show precipitation events which has no correspondence with Mt. Wrangell accumulation events. The black bars show precipitation events which occurred at same timing with Mt. Wrangell accumulation events. Accumulation events at Mt. Wrangell always occurred at same timing with Cordova precipitation events.

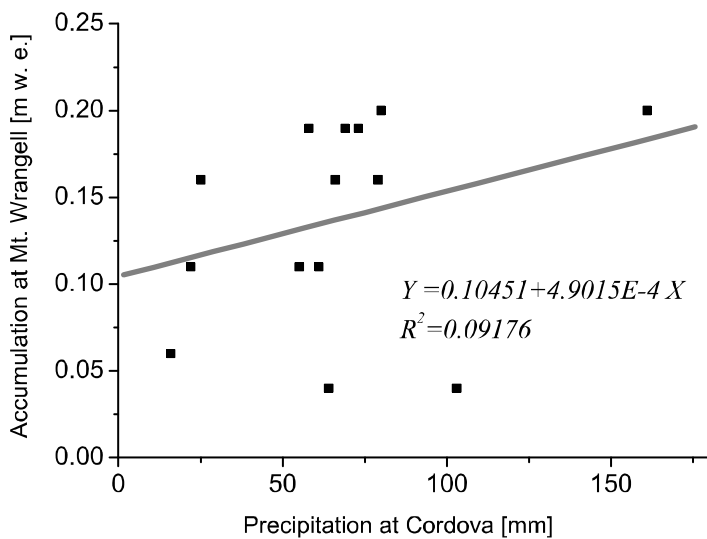


Figure 4.6: Plot of precipitation at Cordova and accumulation at Mt. Wrangell in individual storm events with a regression line (gray line). The accumulation data is converted to water equivalent by the dating (Fig. 3.1).

In a previous study that relates snow accumulation at Mt. Logan to local climate, Rupper et al. [2004] demonstrated that only winters in a high accumulation year have a robust connection with atmospheric circulation. The observed year at Mt. Wrangell is an average accumulation year. However, there still appears to be a simple relationship between snow accumulation at Mt. Wrangell and precipitation at Cordova. The direct relationship between accumulation on Mt. Wrangell and precipitation at a sea-level weather station, lying upwind during storms might be characteristic of Mt. Wrangell only. Snow accumulation at Mt. Wrangell seems to reflect regional weather systems with synoptic scale rather than local convective activity which might be expected for a mountain site.

4.2. Detailed dating of the Mt. Wrangell ice cores

4.2.1. Method

In the Mt Wrangell ice cores, certain dates are known for several depths (Table

4.2). These were used for control points of dating. To interpolate dates between the control points, the relationship between surface condition at the Summit Caldera of Mt. Wrangell and weather station data were used. There are three important results for assuming the dates in the previous subsection;

- 1) surface snow temperature at Mt. Wrangell is well correlated with Gulkana temperature,
- 2) seasonal distribution of accumulation at Mt. Wrangell is similar with that of precipitation at Cordova,
- 3) timing of no accumulation period at Mt. Wrangell correspond to no precipitation or small precipitation event at Cordova.

First, timing of melt event was estimated using the first relation. Daily maximum temperature at Gulkana which exceed 25 °C was considered as potential index of melt event. Melt features in ice cores were dated using this index. Ice lenses and refreezed features of soaked firn in visual stratigraphy were distinguished and the refreezed features of soaked firn was interpreted as surface at the melt events. The dated melt features divide annual layers between summer seasons. Second, daily distribution of accumulation between dated depths was presumed to be same with daily distribution of precipitation at Cordova in corresponding period because of their similarity in seasonality. Dates from this presumption is inaccurate but the difference from the accurate dates should not be large. At least, approximate season should be correct. This assumption was used only as a guide of dating. Third, stepwise changes in density profile which represent boundaries between accumulation events were dated using estimated no accumulation period by Cordova precipitation data. The period that has no precipitation or less than 20 mm in total amount at continuous daily precipitation at

Cordova was considered as no accumulation period at Mt. Wrangell. Length of no accumulation periods were taken account into. Clear stepwise changes which may be formed with wind packing were interpreted as relatively long no accumulation period. Clear dated depths gave feedback to the first step to reduce possible dates of melt features.

Table 4.2: Control depths in dating the Mt. Wrangell ice cores

Date	Descriptions	Depth		
		[m]	[m w. e.]	core
2006/6/22	Surface level at the ice coring in 2006	0.00	0.00	2006-1
2005/6/3	Surface level at the ice coring in 2005	6.48 0.00	2.66 0.00	2006-1 2005b
2004/5/13	Surface level at the ice coring in 2004	12.56 7.57 0.00	5.82 3.25 0.00	2006-2 2005b 2004
2003/6/20	Surface level at the ice coring in 2003	17.00 12.18 5.99 0.00	8.25 5.66 2.42 0.00	2006-2 2005b 2004 2003
2001/4/13	Remarkable spring dust event*	17.20 12.31	8.43 5.66	2004 2003
1992/9/17	Tephra deposition event by a Mt. Spurr eruption*	52.6 47.12	31.0 26.87	2004 2003

*Yasunari et al., 2007

Figure 4.7 shows an example of dating for an annual layer from summer 2004 to summer 2005. There are two control points at the both ends. First, two melt features seems to correspond high temperature events in late June to mid July and early August respectively. Second, cumulative precipitation at Cordova between dated points was fit to depth scale of ice core in water equivalent as a guide of dating. Third, depths of

stepwise changes in detailed density profile was compared with position of precipitation event boundaries in the cumulative precipitation pattern. In this case, stepwise change at 3.5 m w. e. in the 2006 core was remarkable and seemed to fit no precipitation period which indicated in Figure 4.7 at Cordova. The date of this no precipitation event gave date to the Mt. Wrangell 2006 core. This case has tough connection between events in the ice core and at Cordova because both events are remarkable and has no comparable event each other. Other stepwise features in the density profile were also dated by the same way. However, most of the stepwise features and the no precipitation events has a few comparable events each other. In such cases, events in an ice core and Cordova precipitation data were fitted to minimize the number of events that has no comparable events each other.

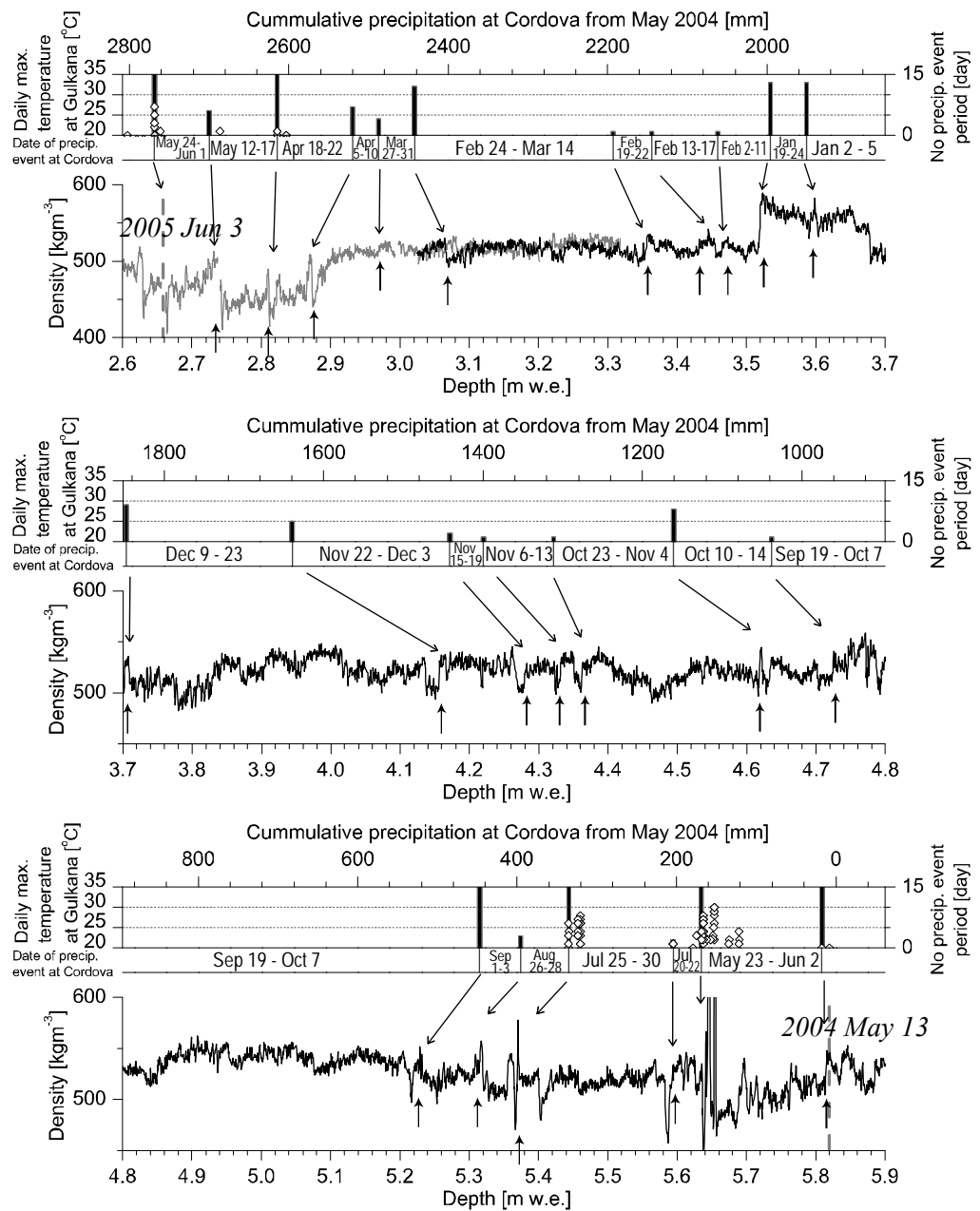


Figure 4.7: Comparison of cumulative precipitation at Cordova and density profile of the Mt. Wrangell ice core for dating. Upper chart: Cumulative precipitation at Cordova from May 2004 to June 2005 (blocks with date) and no precipitation event period (vertical bars). Daily maximum temperature at Gulkana are also shown in same horizontal scale (rhombic plot). Lower chart: Detailed density profile (black solid line) of the Mt. Wrangell 2006-1 core (gray line) and 2006-2 core (black line). Date at two depth are known (vertical break line; see table 4.2 for detail). Stepwise changes in the density profile that are estimated to be formed in no accumulation periods at Mt. Wrangell are connected with no precipitation event at Cordova which is estimated to occur same timing with the events at Mt. Wrangell by arrows. Melt features are connected with high temperature event in the upper chart also by arrows.

For missing values in precipitation data at Cordova, data at Valdez was used after correction using a regression line shown in Figure 4.8. This displacement is reasonable because precipitation data at the two sites is well correlated ($R=0.80$) in daily data (Fig. 4.8) and both Cordova and Valdez shows correspondence in timing of precipitation events with timing of accumulation events at the Summit of Mt. Wrangell.

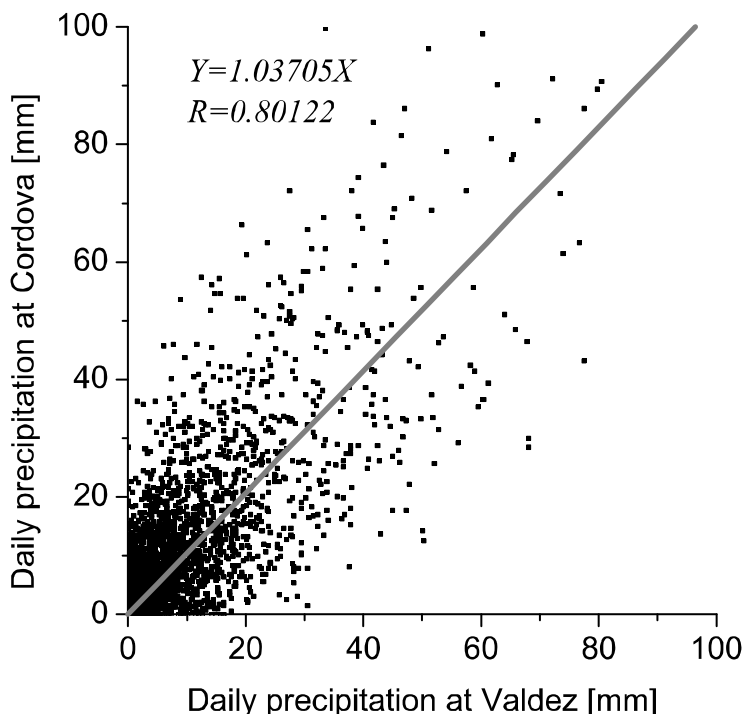


Figure 4.8: Plot of daily precipitation at Valdez and Cordova with a regression line (gray line) and the equation. The plots shows data from 1991 to 2006.

4.2.2. Result and errors

In addition to 5 control points, 30 melt features and 228 accumulation event boundaries appeared as stepwise changes in the detailed density profile were dated for Mt. Wrangell ice cores that cover period from 1991 to 2005. In total, 263 points were dated [See Appendix C for dating points and its descriptions]. It gives 18 dating points

per year in average, which is monthly scale dating. Twenty five events in 30 melt features and 37 events in 228 accumulation event boundaries are reliable in dating because there is no other comparable events in weather station data. Figure 4.9 shows number of melt features in each month. The melt events occurred mainly in June and July. This made dating of summer season reliable. Table 4.2 shows the number of dating points in each year. Although melt events are concentrated in summer, other dating points dispersed in each annual layers and all annual layers have several reliable dating points. Therefore, systematic errors which exceed a few months is hard to occur. The most possible error is caused by mistaking corresponding event at Cordova to adjacent events in unreliable dating points. Figure 4.10 shows spans between adjacent dating points. The most frequent span is 10-15 days and most of spans are within a month. Therefore error in dating is considered to be within a month.

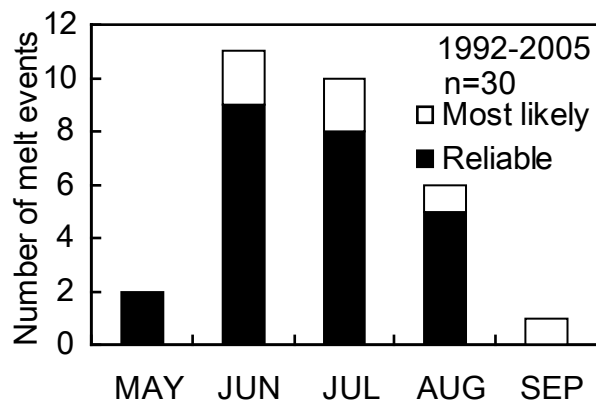


Figure 4.9: Number of melt events that were found in the Mt. Wrangell ice cores from 1992 to 2005 in each month. The event with reliable dating is shown by black bars and with less reliable dating is shown by white bars.

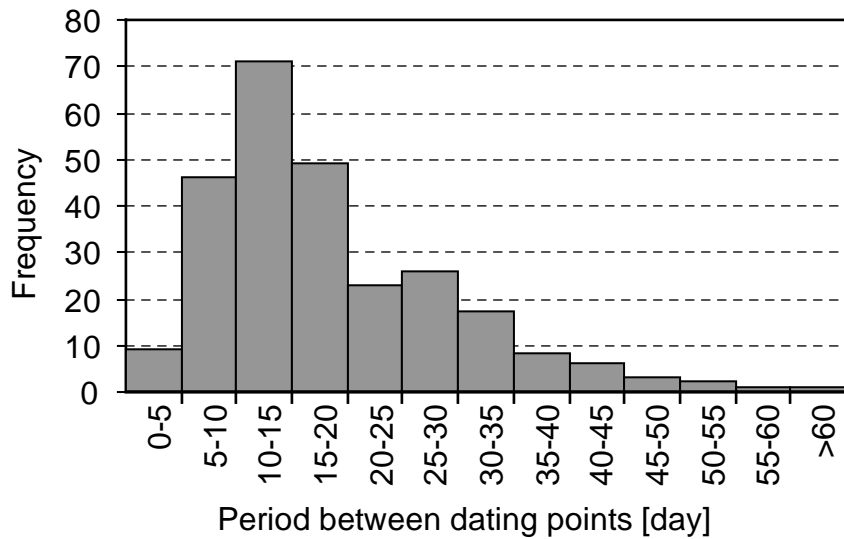


Figure 4.10: Frequency of periods between dating points.

4.3. Monthly variation of parameters in ice core data

4.3.1. Method

The monthly scale dating made it possible to date profile of other parameters such as accumulation rate, stable isotope ratio or tritium concentration. The dated results of these parameters are shown in this subsection. Time axis of ice core parameters was supposed to be liner with water equivalent depth of the core between the dating points. Hydrogen isotope ratio (δD) was analyzed using a mass spectrometer (JASCO International Co. Ltd., Isoprime PyrOH). The estimated measurement error was less than 0.1‰. The sample was taken every 5 cm for the Mt. Wrangell 2006 core and every 10 cm for the other Mt. Wrangell cores (See table 2.1 for ice core information). Tritium was analyzed by a liquid scintillation counter [Yasunari et al., 2007] for the Mt. Wrangell 2003 core.

4.3.2. Result and discussion

Figure 4.11 shows monthly accumulation rate time series from 1992 to 2003 at Mt. Wrangell which is reconstructed using the Mt. Wrangell 2003 core. Likewise the measured result from 2005 to 2006, the highest accumulation rate was seen in late summer to fall in most of years. However, it shows some inter-annual variations. For example, the highest season shift later in 1997 and 2000 and earlier in 1998. It is important to note that a few storm dominate accumulation in a month. In the accumulation measurement (Fig. 4.4), accumulation in 6 months were dominated by 17 storm event. Snow accumulation were detected only on 21 days. Therefore, monthly accumulation rate is highly dependent on number of storm events. This is supposed to be a reason of the inter-annual fluctuation.

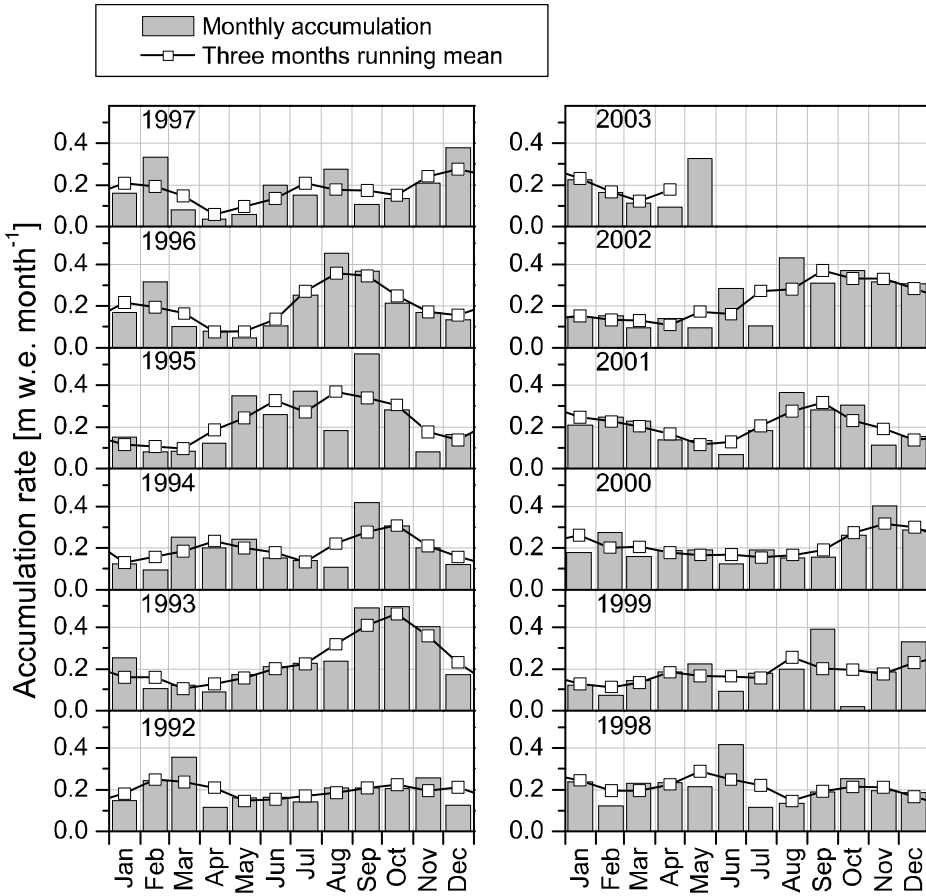


Figure 4.11: Monthly accumulation time series from 1992 to 2003 which is reconstructed from the Mt. Wrangell 2003 core.

Stable isotope ratio fluctuate seasonally in this region and annual maximum has been thought to come summer or warm season [Yasunari et al., 2007; Wake et al., 2002] but calendar date of that had been unknown. Figure 4.12 shows hydrogen isotope ratio (δD) time series from 1992 to 2006. Calendar dates of annual maxima appeared from July to December. Maybe the December peak in 2002 is exceptional because it was an only case that annual maximum appeared after November in the 13 year-record. On the other hand, annual minima were scattered. Cold season which is from November to April seems the range of annual minimum but some minimum peaks appeared in June, July and October. It is important that stable isotope ratio fluctuate largely. It is very often that value of a summer layer is lower than a winter value. Figure 4.13 shows

correlation coefficient between monthly δD and monthly temperature at four weather station shown in table (4stations) from 1991 to 2003. Three month running means were compared because ice core dating may have one month error. The correlations are relatively high from July to November in all four weather station data. Stable isotope data seems to reflect regional temperature from summer to early winter. The relation is unclear in the opposite seasons. Because accumulation in a month is dominated by a few storm events, monthly value in δD represents wet deposition in several days. The higher correlation from summer to early winter might be relate with higher accumulation rate at the season which provide better temporal representation for the atmospheric information.

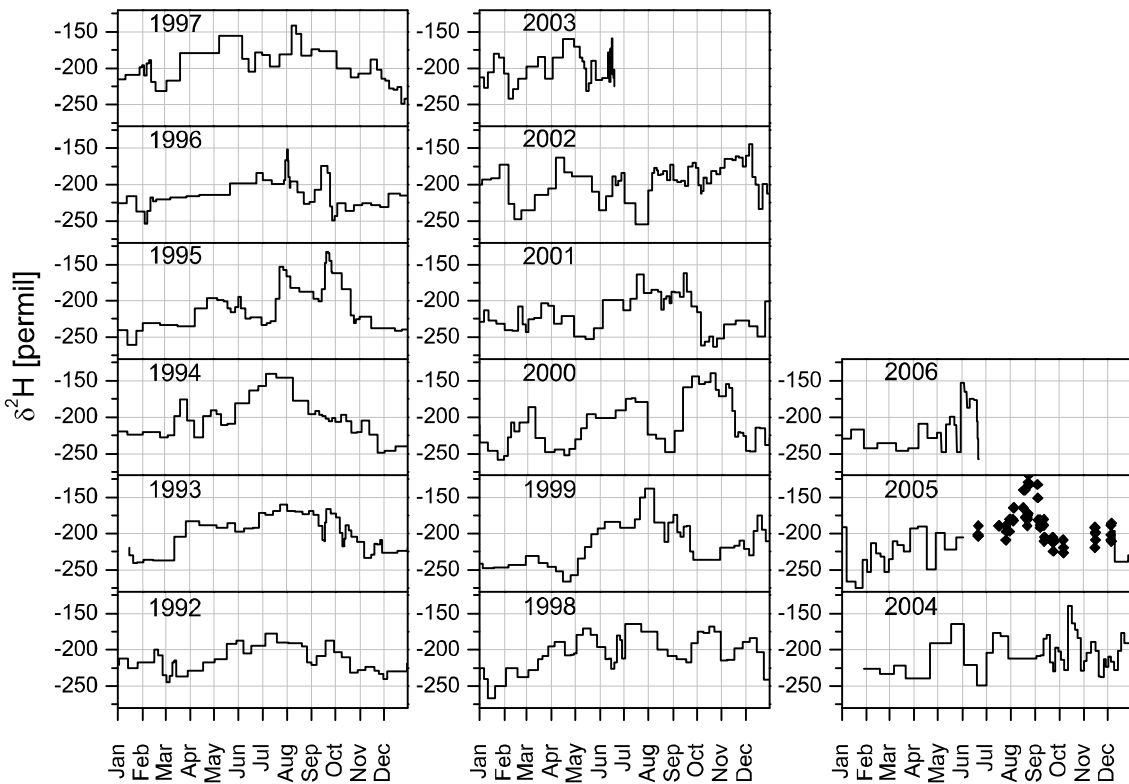


Figure 4.12: Hydrogen isotope ratio time series at Mt. Wrangell. 1992 to 2003: data from the Mt. Wrangell 2003 core [Yasunari et al., 2007], January 2004 to May 2005: data from the Mt. Wrangell 2005a core, June 2005 to June 2006: data from the Mt. Wrangell 2006-1 core.

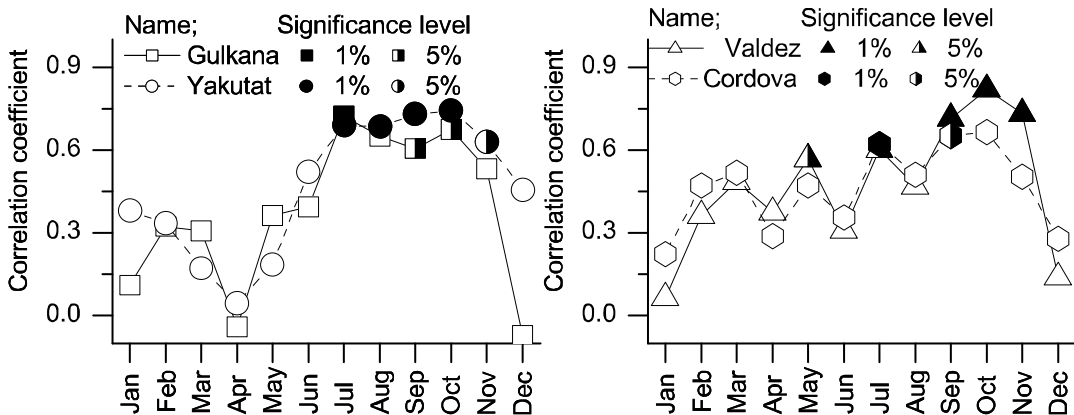


Figure 4.13: Correlation coefficients between three month running mean hydrogen isotopes in ice core data and three month running mean temperature at the four weather stations in south central Alaska (Table 4.1). The correlation coefficients were calculated for each month from 1992 to 2003. Significant correlations are shown with filled marks.

Figure 4.14 shows tritium time series from 1992 to 2003. Annual maximum appeared from March to June each year. Yasunari et al [2007] found annual periodicity of tritium profile and assumed tritium maxima as early spring from relative position of other key parameters. This result agree with the assumption and it is more periodic than accumulation rate distribution or stable isotope ratio. The agreement support validity of dating methods each other.

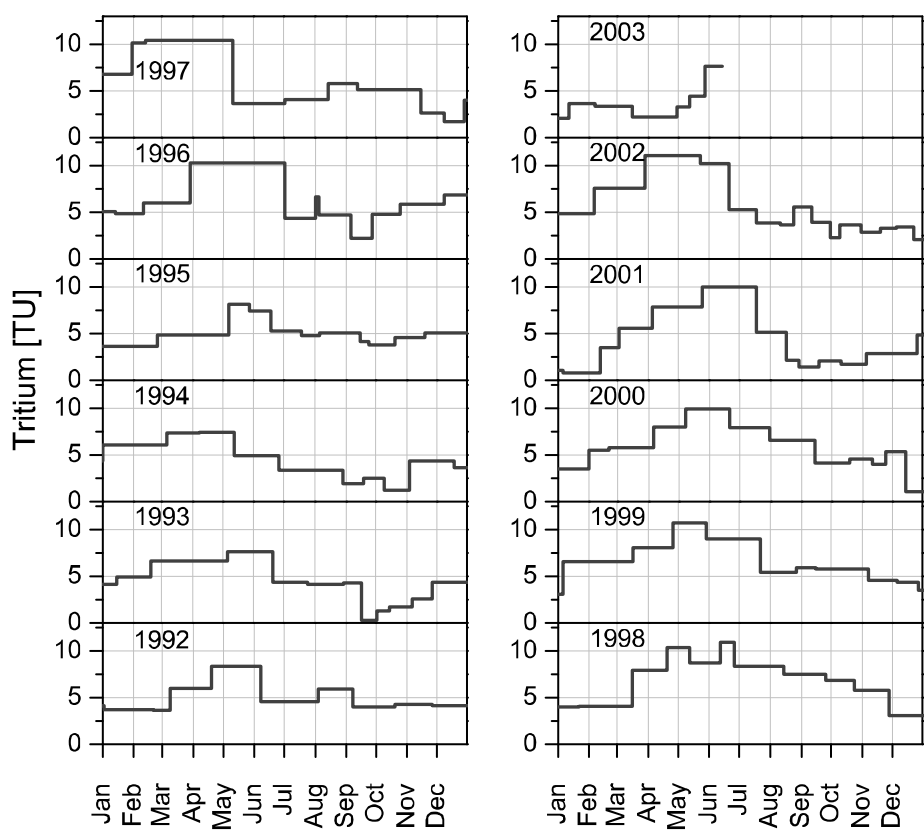


Figure 4.14: Tritium concentration time series at Mt. Wrangell from 1992 to 2003. The original data is presented by Yasunari et al. [2007].

5. Effect of snow drift at alpine ice core sites

Generally, alpine ice core sites suffer from strong wind. In such conditions, precipitated snow is easily removed by snow drifting and/or wind scouring. Fisher et al. [1983] pointed out effect of wind scouring in past climate reconstruction by ice cores in the case of Arctic Canada. Snow drift can remove all of annual snow fall in some cases (e.g. bare ice field in Antarctica [Takahashi et al., 1988]). Rugged topography enhances local gales and redistribution of snow. Hence, relatively gentle topography is preferable for the ice coring to avoid the effect of snow drift. The Summit Caldera of Mt. Wrangell is one of ideal sites at this point because of its wide spread gentle snow field. However, such places are rare in mountains and many ice cores are obtained at saddle locations such as King Col, Mt. Logan because saddle locations tend to have relative thick ice and flat surface, which are essential points to retrieve older ice with less effect of glacier flow and limited on alpine glaciers. In this chapter, the effect of snow erosion was examined by comparison of density profiles and accumulation rate at the King Col, Mt. Logan with those obtained from the Summit Caldera of Mt. Wrangell.

5.1. Comparison of annual accumulation rates

The King Col core is dated using tritium peaks by nuclear test in early 1960s (Fig. 5.1a) and annual layer counting on multi-parameters (Fig. 5.1b) [Goto-Azuma, unpublished data]. Profiles of oxygen isotope ratio and methanesulfonic acid (MSA) are mainly used to determine annual layers.

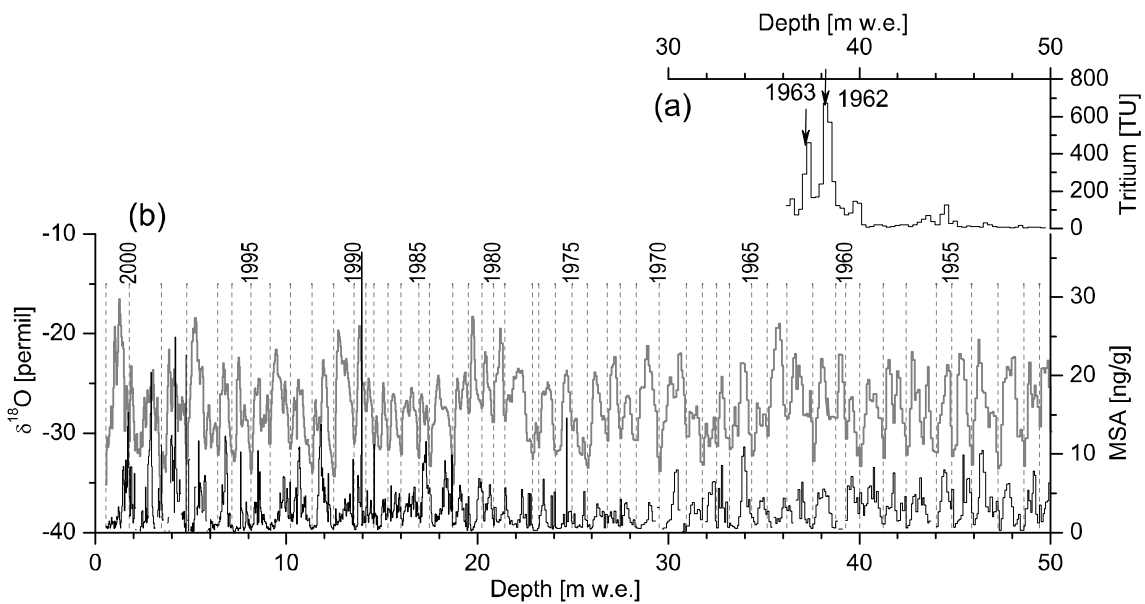


Figure 5.1: Ice core parameters and assumed dates at certain depths of the King Col core. (a) Tritium profile. The peaks by nuclear tests determine the dates as 1962 and 1963. (b) Oxygen isotope ratio (thick gray line), MSA (thin black line) and assumed year of accumulation. Annual minima of oxygen isotope ratio are taken as annual layer boundaries (vertical break line) [Goto-Azuma et al., unpublished data].

Annual minima of oxygen isotope were taken as annual layer boundaries. Annual accumulation time series for 30 years at King Col and that of Mt. Wrangell 2003 core site determined by annual isotope minima [Yasunari et al., 2007] are compared (Fig. 5.2a). The effect of ice deformation is negligible because the corresponding layers are firm layers. Hence annual layer thicknesses are considered as annual net balance, which is close to annual accumulation rate at those sites. Averaged annual net balance is 1.1 m w. e. a^{-1} at King Col and 2.5 m w. e. a^{-1} at the Mt. Wrangell 2003 core site. Standard deviation of the annual accumulation time series is 0.33 m w. e., 36% of the average for the King Col data and is 0.47 m w. e., 19% of the average for the Mt. Wrangell data. The dating method by stable isotope ratio made inter-annual variation of the Mt. Wrangell ice core larger than the accumulation rate presented in Fig. 4.11 (Figure 5.2b). However, it is much smaller than the King Col data in fraction to the average.

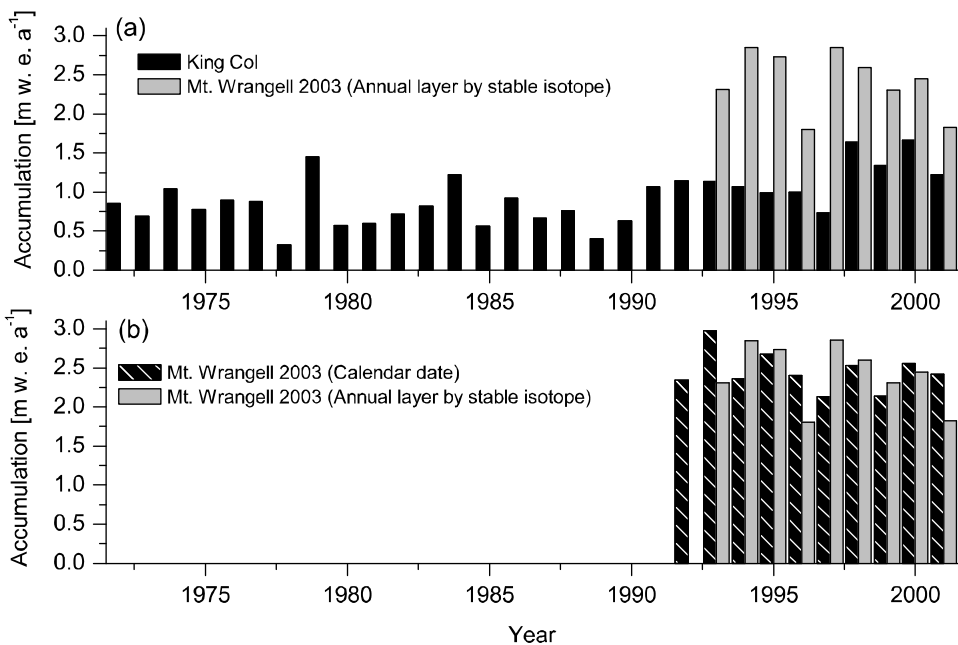


Figure 5.2: (a) Annual accumulation time series at the King Col (black bars) and the Mt. Wrangell 2003 core site (gray bars). Each annual layer is determined by annual minimum peak of stable isotope ratio. (b) Annual accumulation time series at the Mt. Wrangell 2003 core site determined by stable isotope peaks (gray bars) and calendar date (black bars with white lines) that is presented in Figure 4.11.

Annual layer thicknesses are especially thin in 1977 (0.32 m w. e.) and 1988 (0.40 m w. e.) in the King Col data. The density profile is compared with seasonal fluctuation of the oxygen isotope ratio and MSA around 1977 (Fig. 5.3) and 1988 (Fig. 5.4). Stepwise change with rectangular shape in density profile implies successive erosion and the series of such features have a high proportion in the 1977 and 1988 layers. In addition, MSA profile has no peak in the 1977 layer but oxygen isotope minimum has a peak at the same depth in the 1988 layer. Peak of MSA appears in summer between two successive stable isotope minima at King Col in usual year (Fig. 5.1). These correspondences in the ice core parameters suggest that the annual layer counting is reasonable and large fraction of annual snow disappeared in 1977 and 1988 by erosion events. Larger variation of annual accumulation rate in King Col than Mt. Wrangell is

not because of variation in snow precipitations but of irregular erosion events.

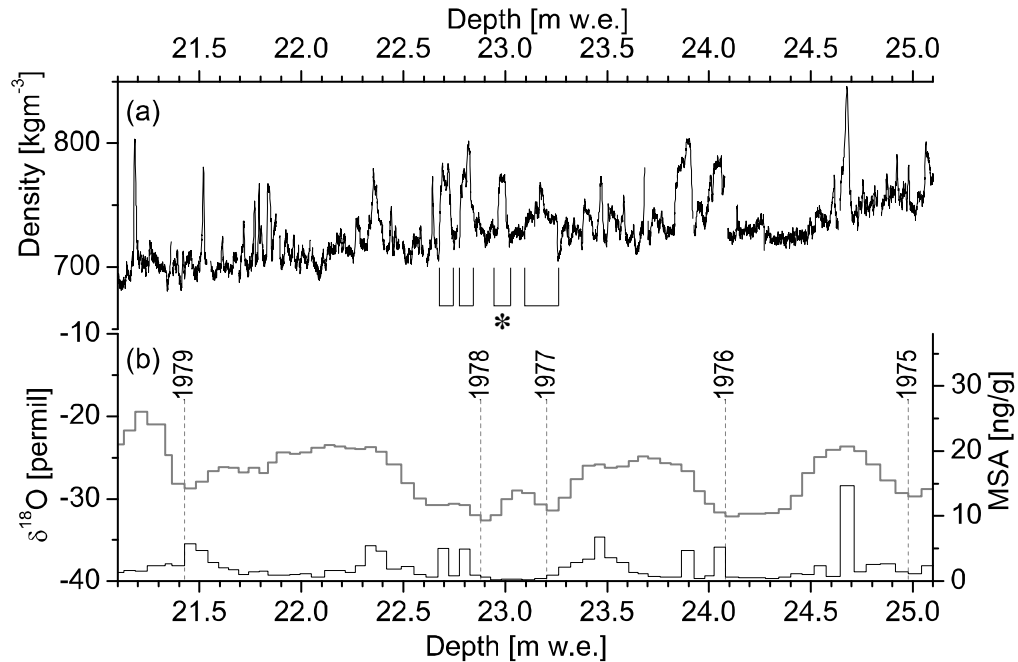


Figure 5.3: Parameters of the King Col core around 1977. (a) Density profile. Marked range by an asterisk indicate part of relative high density associated with stepwise change, which implies erosion event. (b) Oxygen isotope (thick line) and MSA (thin line) profiles with annual layer boundaries (vertical break line) which was determined by annual isotope minima.

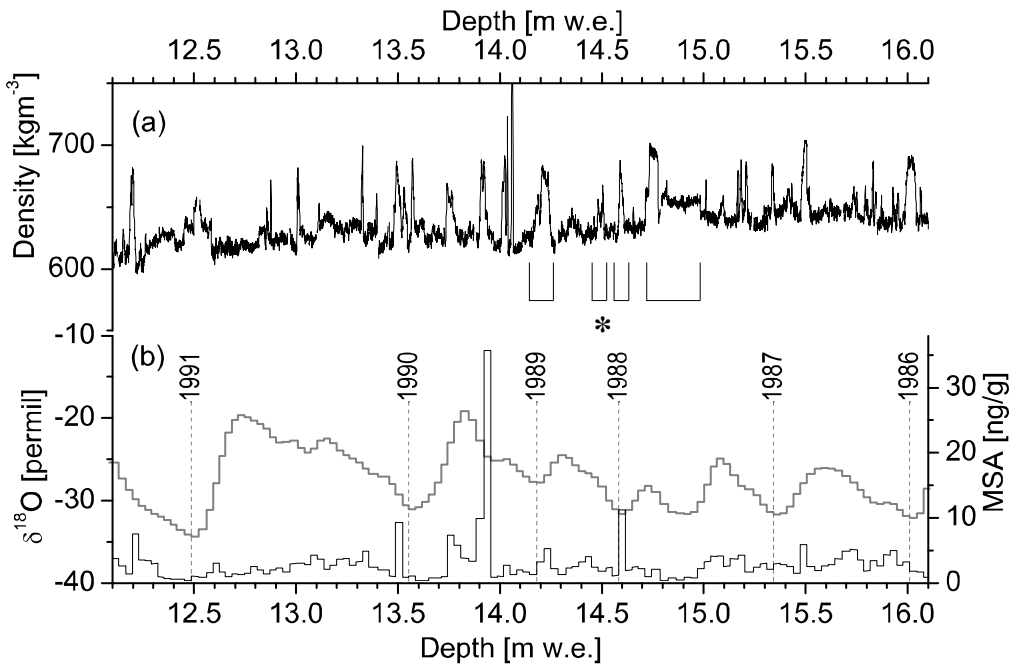


Figure 5.4: Parameters of the King Col core around 1988. (a) Density profile. Marked range by an asterisk indicate part of relative high density associated with stepwise change, which implies erosion event. (b) Oxygen isotope (thick line) and MSA (thin line) profiles with annual layer boundaries (vertical break line) which was determined by annual isotope minima.

5.2. Effect of erosions to ice core parameters

Fisher and Koerner [1994] explained that difference of oxygen isotopes in the multiple ice cores drilled on the Agassiz Ice Cap was caused by snow-drifting and wind-scouring of winter snow. There are similar examples in the profile of King Col core. From 1979 to 1982, annual minima of oxygen isotope ratio are higher than other years (Fig. 5.1b). At the corresponding part, the density is relatively higher and it implies occurrences of erosion events (Fig. 5.5). Although stable isotope ratio is considered to reflect regional air temperature, there is no tendency that temperatures were particularly higher than other years at the period at Yakutat, the closest weather station from Mt. Logan. (Fig. 5.6). Therefore it is reasonable to speculate that there was

no temperature shift at the King Col in the period. Hence the higher annual minima of oxygen isotope ratio than usual years are the indication of winter erosion. Density profile is thus useful proxy for the past erosion events to test validity of other ice core parameters such as stable isotope ratio.

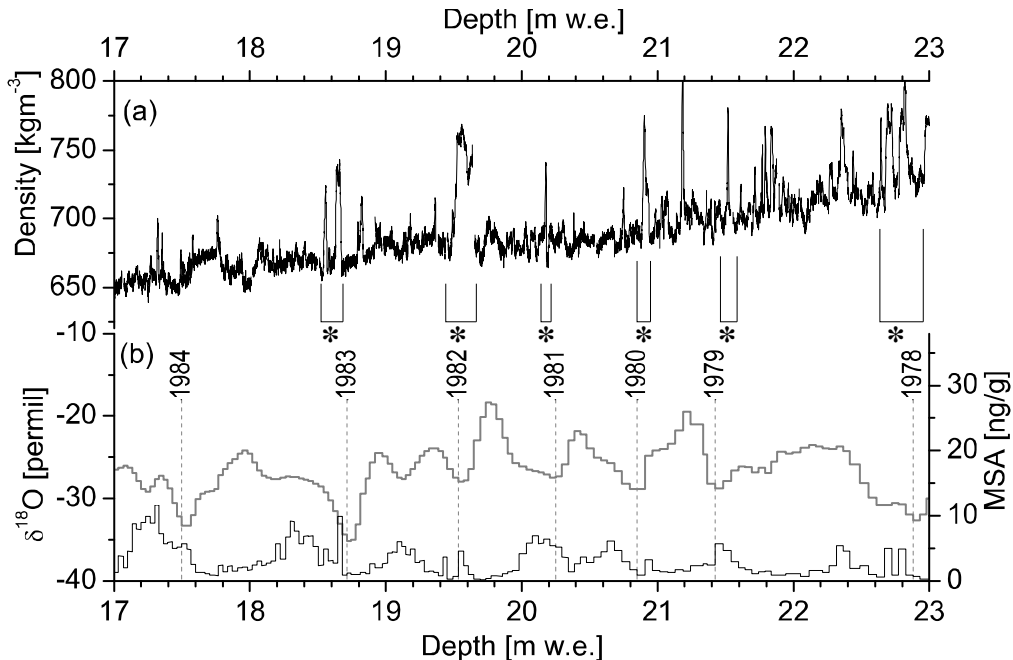


Figure 5.5: Parameters of the King Col core from 1978 to 1984. (a) Density profile. Marked range by asterisk indicate relative high density associated with stepwise change occurred with annual oxygen isotope minimum. (b) Oxygen isotope (thick line) and MSA (thin line) profiles with annual layer boundaries (vertical break line) which was determined by annual isotope minima.

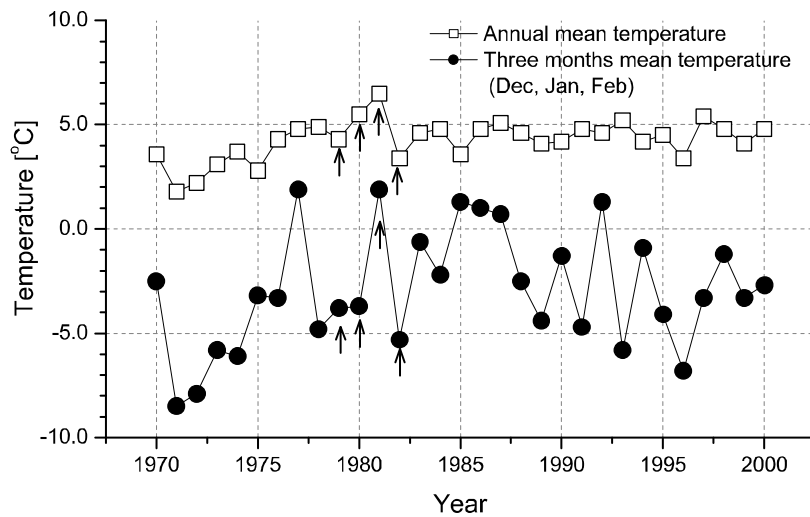


Figure 5.6: Annual mean temperature (white square) and mean three months temperature from December to February (black circle) at Yakutat for 30 years. Arrows indicate years with relatively high annual minima in oxygen isotope ratio shown in Figure 5.5.

5.3. Bending in depth-density profile

The bending in the density profile of the King Col core (Fig. 2.11) is characterized by relatively high density layers associated with step wise changes. Standard deviation of density decreases with increasing depth under normal condition. Mt. Wrangell is a typical case of that (Fig. 5.7a and 5.7b). Except the melt features, standard deviation of density decreased toward depth. On the other hand, the standard deviation of density has second peak at 25 m w. e. in the King Col profile (Fig. 5.7d). The depth correspond to the depth of bending in the density curve (Fig 2.11 and Fig. 5.7c). The bending and second peak of the standard deviation seems to be caused by sudden increase in density profile associated with series of stepwise changes (Fig. 5.7e and 5.7f). Remarkable erosion events were expected at the depths. Such bending feature in density curve is supposed to be an indicator of remarkable erosion events.

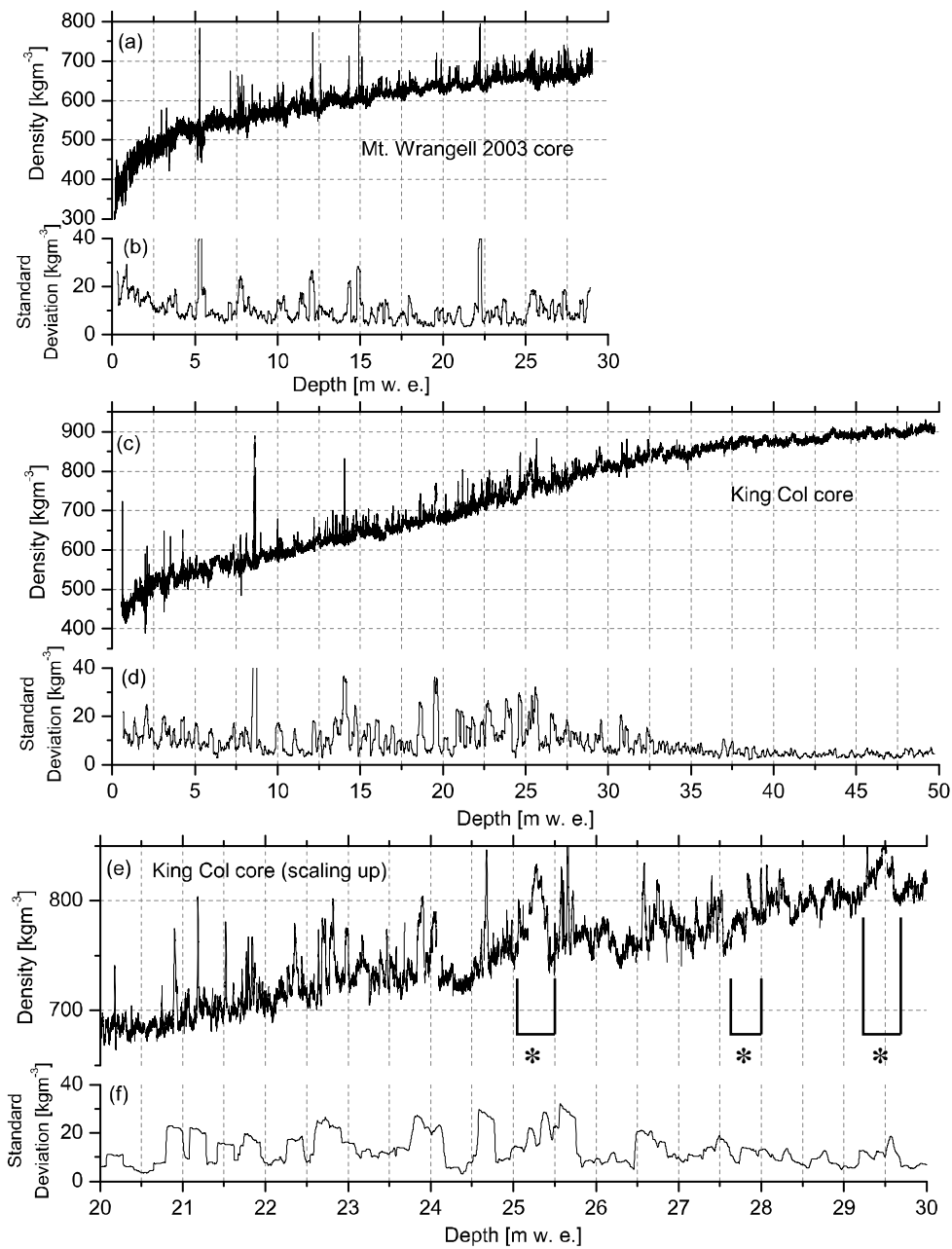


Figure 5.7: Depth-density profiles in water equivalent depth and 0.2 m w.e. -running standard deviation of density. (a) and (b) Mt. Wrangell 2003 core; (c) and (d) King Col core; (e) and (f) King Col core with scaling up. Asterisks shows series of stepwise changes in the density profile which forms remarkably denser layer than the shallower part.

5.4. Redistribution of accumulated snow at the Summit Caldera of Mt. Wrangell

In the Summit Caldera of Mt. Wrangell, the 1982 core site at north side has much less accumulation than the center (Fig. 2.3). Figure 5.8 shows picture of the

Summit Caldera from the summit just after a windy storm event in June 2006. A series of dune was formed by wind over the saddle between the summit and the North crater (Fig. 5.8a). This patterned surface was most clearly seen at the 1982 core site (Fig. 5.8b). However, the intensity of this pattern becomes small toward the center of the caldera and the surface becomes smooth at the 2006 camp/core site (Fig. 5.9c). The distribution pattern of dunes suggests that accumulated snow is eroded then redistributed toward the center of the caldera, which is well agreed with actual accumulation distribution.

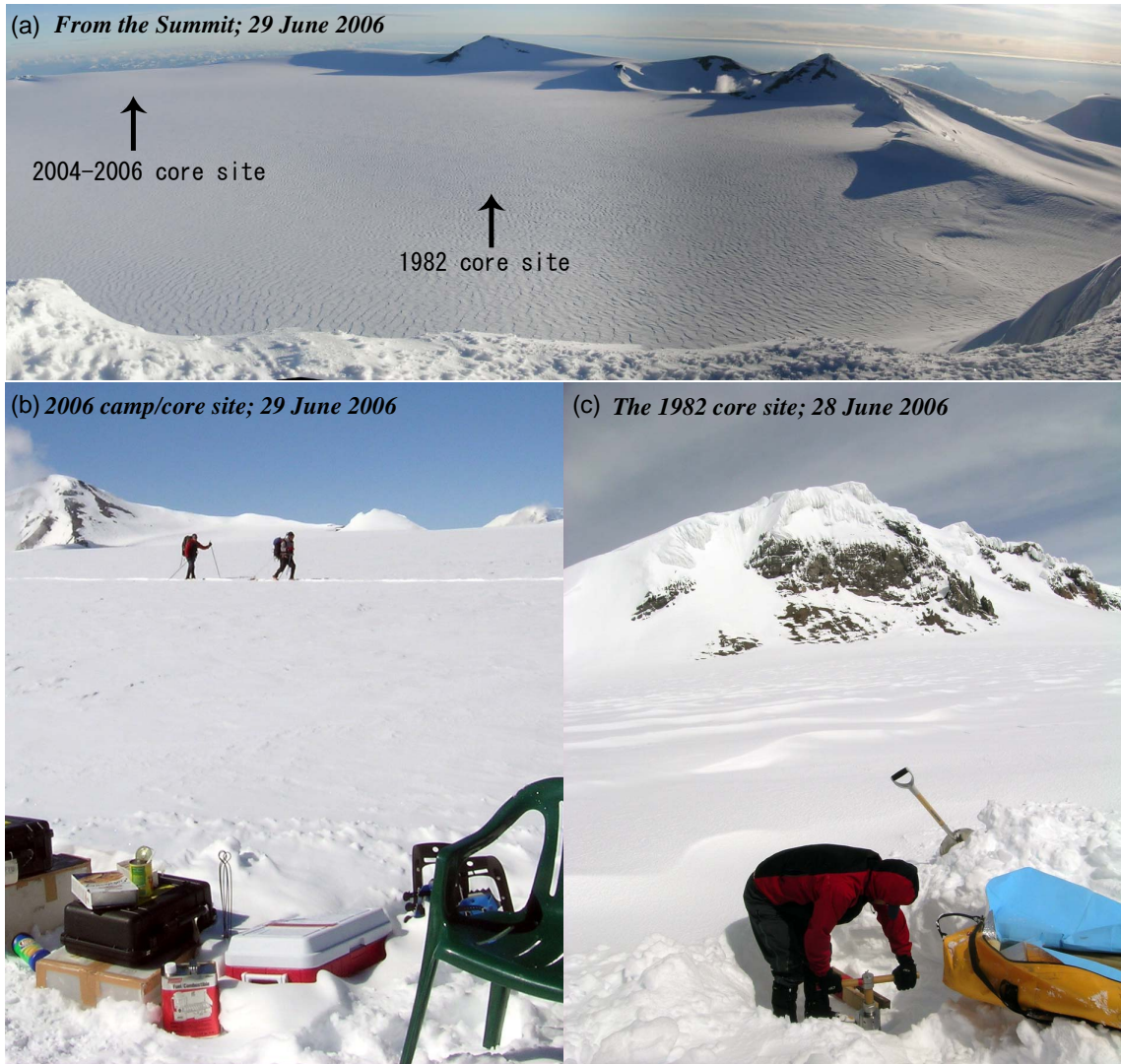


Figure 5.8: Pictures of the Summit Caldera, Mt. Wrangell on June 2006. (a) view from the summit of Mt. Wrangell. (b) camp site. The ice core sites in 2004, 2005, 2006 are located within several tens meters. (c) The 1982 core site close to the north rim.

6. Conclusions

6.1. Interpretation of detailed density profiles as past surface condition proxy data

An 8.33 m-depth firn core, which correspond to more than a full year was drilled at the Summit Caldera of Mt. Wrangell in June 2006. In situ temperature and snow accumulation measurement was carried out from June 2005 to June 2006 was successful. Detailed density profile and stratigraphy of the core was compared with the snow accumulation history. As the result, stepwise changes in the density profile were interpreted as accumulation free periods and rectangular shapes of the density profile were interpreted as erosion events at the surface. These kinds of characteristic shapes in density profiles were maintained in the ice cores drilled in 2003, 2004, 2005 and 2006 at the Summit Caldera of Mt. Wrangell density ranges of which were less than 700 kgm^{-3} .

6.2. Detailed dating using density profiles

The results of in situ temperature and snow accumulation at the Summit Caldera of Mt. Wrangell for one year was correlated with regional weather stations in South Central Alaska. 1)Hourly surface snow temperature at Mt. Wrangell was correlated with hourly air temperature at Gulkana. This made it possible to date timing of surface melt event at Mt. Wrangell from air temperature data at Gulkana for the past. 2)Timing of precipitation free periods at Cordova were same as timing of accumulation free period or erosion event at Mt. Wrangell. This made it possible to date stepwise changes and rectangular shapes of density profiles for the past. 3)Seasonal precipitation distribution at Cordova was similar with seasonal accumulation distribution at Mt. Wrangell. This made it possible to estimate seasonal accumulation distribution for the

past. As the results, Mt. Wrangell ice cores were dated with monthly temporal scale from 1991 to 2005. Averaged number of dating points were 18 in an annual layer.

According to the monthly scale dating, variation of accumulation rate, stable isotope ratio and tritium became clear. Although there were inter annual variations, accumulation rate were higher in fall season. Annual maxima of stable isotope peaks appeared from July to December. Annual tritium peaks were appeared from March to June.

6.3. Accumulation environment of alpine ice core sites

Detailed density profile of the King Col core was examined and compared with that of the Mt. Wrangell core. Seasonal variations of stable isotope ratio and MSA profile of the King Col core were unclear at certain depths. Frequent rectangular shapes in the density profile suggest that it was because of erosion events. The frequent rectangular shape also made a bending in the depth-density curve in larger view. These results and relative large variation of accumulation rate to the Mt. Wrangell implies saddle locations in alpine ice core sites are affected by erosions. This effect should be taken into account for interpretations.

6.4. Meaning of this study

The most important result of this study is monthly scale dating of the ice core. Probably, this is the highest time resolution of ice core dating in the current ice core studies. Although this dating method is limited to the period that weather station data is available, which is past 100 years, it is still very important result because alpine ice core records what sea level weather station never records in the past such as past transported

materials in atmospheric circulation or past climate proxy at free troposphere. This study made it possible to connect such important information from the alpine ice core to other observed record and/or model results in future study.

Reference

- Akitaya, E., and T. Yamada (1991), Snow survey (in Japanese), in *Survey methods for snow and ice (in Japanese)*, edited by Japanese Society of Snow and Ice, pp. 29-45, Hokkaido University Press, Sapporo.
- Bader, H. (1954), Sorge's Law of densification of snow on high polar glaciers, *Journal of Glaciology*, 2(15), 319-323.
- Benson, C. S. (1962), Stratigraphic studies in the snow and firn of the Greenland Ice Sheet, *SIPRE Research Report*, 70.
- Benson, C., S. (1968), Glaciological studies on Mount Wrangell, Alaska, 1961, *Arctic*, 21(3), 127-152.
- Benson, C. S., and R. J. Motyka (1978), Glacier-volcano interactions on Mount Wrangell, Alaska, *Annual Report, Geophysical Institute, University of Alaska*, pp. 1-25.
- Benson, C., S. (1984), Ice core drilling at Mt. Wrangell, Alaska. 2nd International Workshop/Symposium on Ice Drilling Technology, *CRREL Special report*, 84(34), 61-68.
- Benson, C., and A. Follett (1986), Application of photogrammetry to the study of volcano-glacier Interactions on Mount Wrangell, Alaska, *Photogrammetric Engineering And Remote Sensing*, 52(6), 813-827.
- Benson, C., et al. (2007), Glacier-volcano interactions in the North Crater of Mt Wrangell, Alaska, *Annals of Glaciology*, 45, 48-57.
- Clarke, G., et al. (1989), Radar imaging of glaciovolcanic stratigraphy, Mount Wrangell caldera, Alaska - Interpretation model and results, *Journal of Geophysical Research-Solid Earth and Planets*, 94(B6), 7237-7249.
- Dansgaard, W., et al. (1993), Evidence for general instability of past climate from a 250-kyr ice-core record, *Nature*, 364(6434), 218-220.
- Devaux, J. (1933), L'économie radio-thermique des champs de neige et des glaciers, *Annales de physique. Ser. 10, 20*, 5-67.
- Fisher, D. A., et al. (1983), Effect of wind scouring on climatic records from ice-core oxygen-isotope profiles, *Nature*, 301(5897), 205-209.
- Fisher, D. A., and R. M. Koerner (1994), Signal and noise in four ice-core records from the Agassiz Ice Cap, Ellesmere Island, Canada: details of the last millennium for stable isotopes, melt and solid conductivity, *The Holocene*, 4(2), 113-120.

- Fisher, D. A., et al. (2004), Stable isotope records from Mount Logan, Eclipse ice cores and nearby Jellybean Lake. Water cycle of the North Pacific over 2000 years and over five vertical kilometres: Sudden shifts and tropical connections, *Géographie physique et Quaternaire*, 58(2-3), 337-352.
- Gerland, S., et al. (1999), Density log of a 181 m long ice core from Berkner Island, Antarctica, *Annals of Glaciology*, 29, 215-219.
- Goto-Azuma, K., et al. (2003), An overview of the Japanese glaciological studies on Mt. Logan, Yukon Territory, Canada in 2002, *Bulletin of Glaciological Research*, 20, 65-72.
- Herron, M. M., and C. C. Langway (1980), Firn densification - an empirical-model, *Journal of Glaciology*, 25(93), 373-385.
- Holdsworth, G. H., et al. (1992), Ice core climate signals from Mount Logan, Yukon A.D. 1700-1987, in *Climate Since A.D. 1500*, edited by R. S. a. J. Bradley, Philip D., pp. 483-504, Routledge, London.
- Hori, A., et al. (1999), A detailed density profile of the Dome Fuji (Antarctica) shallow ice core by X-ray transmission method, *Annals of Glaciology*, 29, 211-214.
- Jun, L., and H. J. Zwally (2002), Modeled seasonal variations of firn density induced by steady-state surface air-temperature cycle, in *Annals of Glaciology*, 34, 299-302
- Kang, S., et al. (2005), A 290-a record of atmospheric circulation over the North Pacific from a Mt. Logan ice core, Yukon Territory, *Acta Oceanologica Sinica*, 24(4), 81-90.
- Koerner, R. M., and S. Ohio State University. Institute of Polar (1971), *A stratigraphic method of determining the snow accumulation rate at Plateau Station, Antarctica, and application to South Pole-Queen Maud Land traverse 2, 1965-1966*, Ohio State University, Institute of Polar Studies, Columbus, OH.
- Kohshima, S., et al. (2002), Ice core drilling on Southern Patagonia Icefield -Development of a new portable drill and the field expedition in 1999, *Memoirs of National Institute of Polar Research. Special issue*, 56, 49-58.
- Maeno, N., and T. Kuroda (1986), Structures and properties of snow and ice (in Japanese), pp. 143-148, Kokon-shoin, Tokyo.
- Greenland Ice-core Project Members (1993), Climate instability during the last interglacial period recorded in the GRIP ice core, *Nature*, 364(6434), 203-207.
- Nakazawa, F., et al. (2005), Dating of seasonal snow/firn accumulation layers using pollen analysis, *Journal of Glaciology*, 51(174), 483-490.

- Partington, K. (1998), Discrimination of glacier facies using multi-temporal SAR data, *Journal Of Glaciology*, 44(146), 42-53.
- Paterson, W. S. B. (1994), *The Physics of Glaciers*, Third edition ed., Butterworth Heinemann, Oxford.
- Petit, J. R., et al. (1999), Climate and atmospheric history of the past 420,000 years from the Vostok ice core, Antarctica, *Nature*, 399(6735), 429-436.
- Rupper, S., et al. (2004), The relationship between snow accumulation at Mt. Logan, Yukon, Canada, and climate variability in the North Pacific, *Journal of Climate*, 17(24), 4724-4739.
- Schwikowski, M., et al. (1999), A high-resolution air chemistry record from an Alpine ice core: Fiescherhorn glacier, Swiss Alps, *Journal of Geophysical Research-Atmospheres*, 104(D11), 13709-13719.
- Shiraiwa, T., et al. (2001), Characteristics of a crater glacier at Ushkovsky volcano, Kamchatka, Russia, as revealed by the physical properties of ice cores and borehole thermometry, *Journal of Glaciology*, 47(158), 423-432.
- Shiraiwa, T., et al. (2003), Ice core drilling at King Col, Mount Logan 2002, *Bulletin of Glaciological Research*, 20, 57-63.
- Shiraiwa, T., et al. (2004), Shallow ice-core drilling at Mount Wrangell, Alaska, *Bulletin of Glaciological Reaserch*, 21, 71-77.
- Takahashi, A. (1996), Development of a new shallow ice core drill (in Japanese), *Seppyo*, 58(1), 29-37.
- Takahashi, S., et al. (1988), A bare ice field in East Queen Maud Land, Antarctica, caused by horizontal divergence of drifting snow, *Annals of Glaciology*, 11, 156-160.
- Thompson, L., et al. (1984), El-Nino southern oscillation events recorded in the stratigraphy of the tropical Quelccaya ice cap, Peru, *Science*, 226(4670), 50-53.
- Wake, C., et al. (2002), The climate signal recorded in the oxygen-isotope, accumulation and major-ion time series from the Eclipse ice core, Yukon Territory, Canada, *Annals of Glaciology*, 35, 416-422.
- Watanabe, O., et al. (1999), The paleoclimate record in the ice core at Dome Fuji station, East Antarctica, in *Annals of Glaciology*, 29, 176-178.
- Yalcin, K., et al. (2006), A 1000-yr record of forest fire activity from Eclipse Icefield, Yukon, Canada, *The Holocene*, 16(2), 200-209.

Yasunari, T., et al. (2007), Intra-annual variations in atmospheric dust and tritium in the North Pacific region detected from an ice core from Mount Wrangell, Alaska, *Journal of Geophysical Research-Atmospheres*, 112(D10), D10208, DOI:10.1029/2006JD008121.

Zagorodnov, V., et al. (2005), Intermediate-depth ice coring of high-altitude and polar glaciers with a lightweight drilling system, *Journal of Glaciology*, 51(174), 491-501.

Zwally, H. J., and L. Jun (2002), Seasonal and interannual variations of firn densification and ice-sheet surface elevation at the Greenland summit, *Journal of Glaciology*, 48(161), 199-207.

Appendix A

Detection of snow burial dates at the snow accumulation measurement

Appendix A shows temperature profiles on the accumulation measurement with descriptions of detected events. Snow burial events, re-exposed events and melt events of temperature sensors at certain heights were detected from their temperature profiles.

Heights of each sensors are expressed as height from surface level on 3 June 2005.

June 2005

The sensor at 0.24 m-high assumed to be buried on 19 June because amplitude of diurnal fluctuation had been smaller after that (Fig. A.1a).

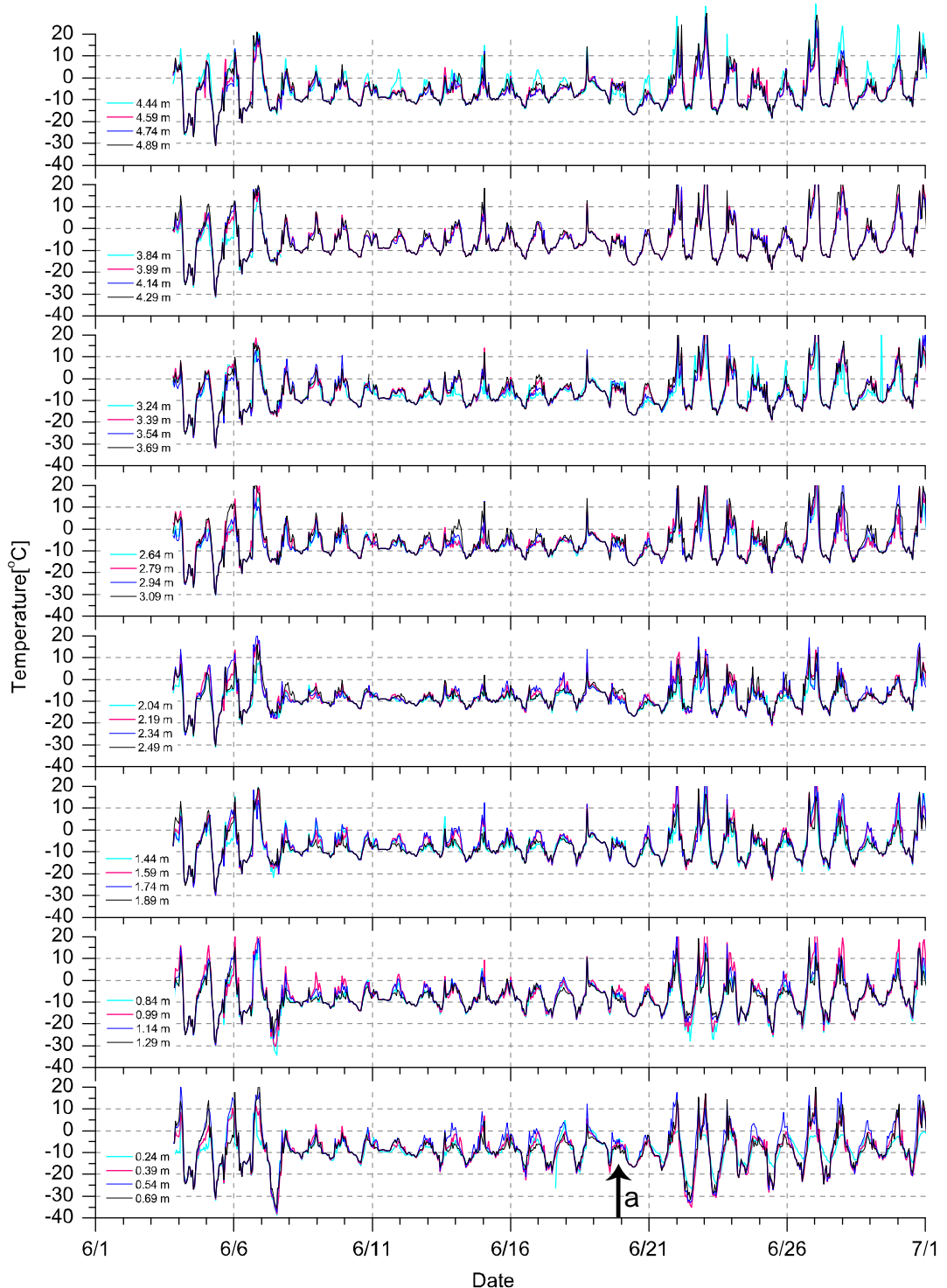


Figure A.1: Temperature profiles at every 0.15 m height on the accumulation measurement tower in June 2005. See main text for descriptions about arrows.

July 2005

The sensor at 0.39 m-high assumed to be buried on 17 July because amplitude of

diurnal fluctuation had been smaller after that than other exposed sensors above (Fig. A.2a).

The sensor at 0.69 m-high assumed to be buried on 26 July because amplitude of diurnal fluctuation had been smaller after that than other exposed sensors above (Fig. A.2b).

The sensors at 0.84 m-high and 0.99 m-high assumed to be buried on 31 July because amplitude of diurnal fluctuation had been smaller after that than other exposed sensors above (Fig. A.2c; Fig. A.3).

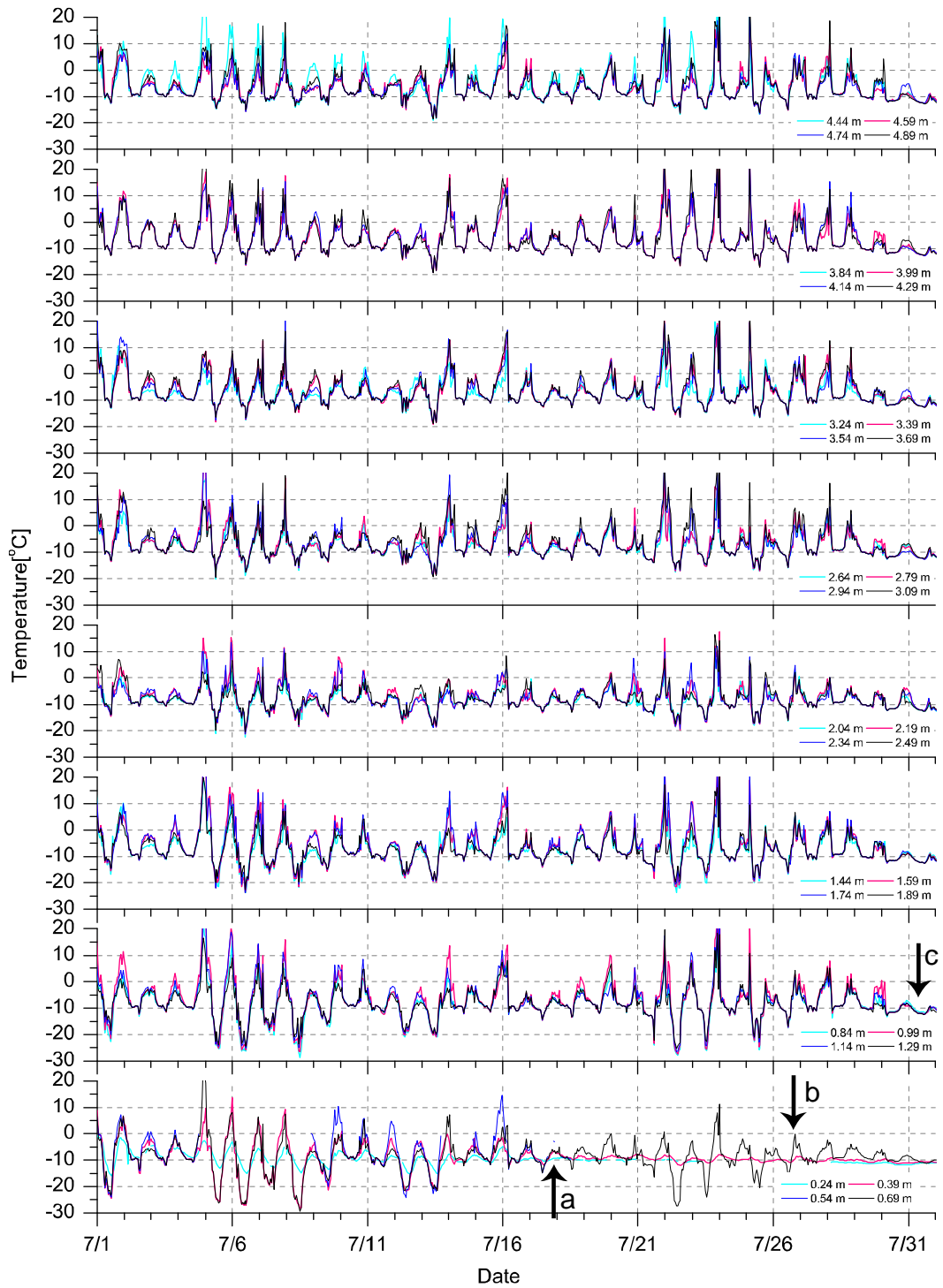


Figure A.2: Temperature profiles at every 0.15 m height on the accumulation measurement tower in July 2005. See main text for descriptions about arrows.

August 2005

The sensor at 1.14 m-high assumed to be buried on 1 August because amplitude of

diurnal fluctuation had been smaller after that than other exposed sensors above (Fig. A.3a).

The sensor at 1.29 m-high assumed to be buried on 4 August because amplitude of diurnal fluctuation had been smaller after that than other exposed sensors above (Fig. A.3b).

The sensor at 1.44 m-high assumed to be buried on 5 August because amplitude of diurnal fluctuation had been smaller after that than other exposed sensors above (Fig. A.3c).

The sensor at 1.44 m-high assumed to be exposed again on 7 August because amplitude of diurnal fluctuation had became similar with exposed sensor above after that (Fig. A.3d).

The sensor at 1.29 m-high assumed to be exposed again on 9 August because amplitude of diurnal fluctuation had became similar with exposed sensor above after that (Fig. A.3e).

The sensor at 1.14 m-high assumed to be exposed again on 10 August because the daily maximum temperature was higher than melting point (Fig. A.3f).

The sensor at 0.99 m-high assumed to be exposed again on 11 August because the daily maximum temperature was higher than melting point (Fig. A.3g).

Melt events occurred at daytime from 11 to 14 August Some of buried sensors had recorded melt points (0.99m-high:11 Aug.; 0.84 m-high:12 Aug.-14 Aug.; 0.69m-high: Aug.12).

The sensor at 0.84m-high assumed to be exposed again on 15 August because the daily maximum temperature slightly exceeded melting point (Fig. A.3h).

The sensor at 0.84m-high assumed to be buried again on 17 August because amplitude

of diurnal fluctuation had been smaller after that than exposed sensors above (Fig. A.3i).

The sensors at 0.99m-high, 1.14m-high, 1.29 m-high, 1.44m-hgih and 1.59m-high assumed to be buried on 21 August because amplitude of diurnal fluctuation had been smaller after that than exposed sensors above (Fig. A.3j).

The sensors at 1.74m-high and 1.89m-high assumed to be buried on 23 August because amplitude of diurnal fluctuation had been smaller after that than exposed sensors above (Fig. A.3k).

The sensor at 2.04m-high assumed to be buried on 25 August because amplitude of diurnal fluctuation had been smaller after that than exposed sensors above (Fig. A.3l).

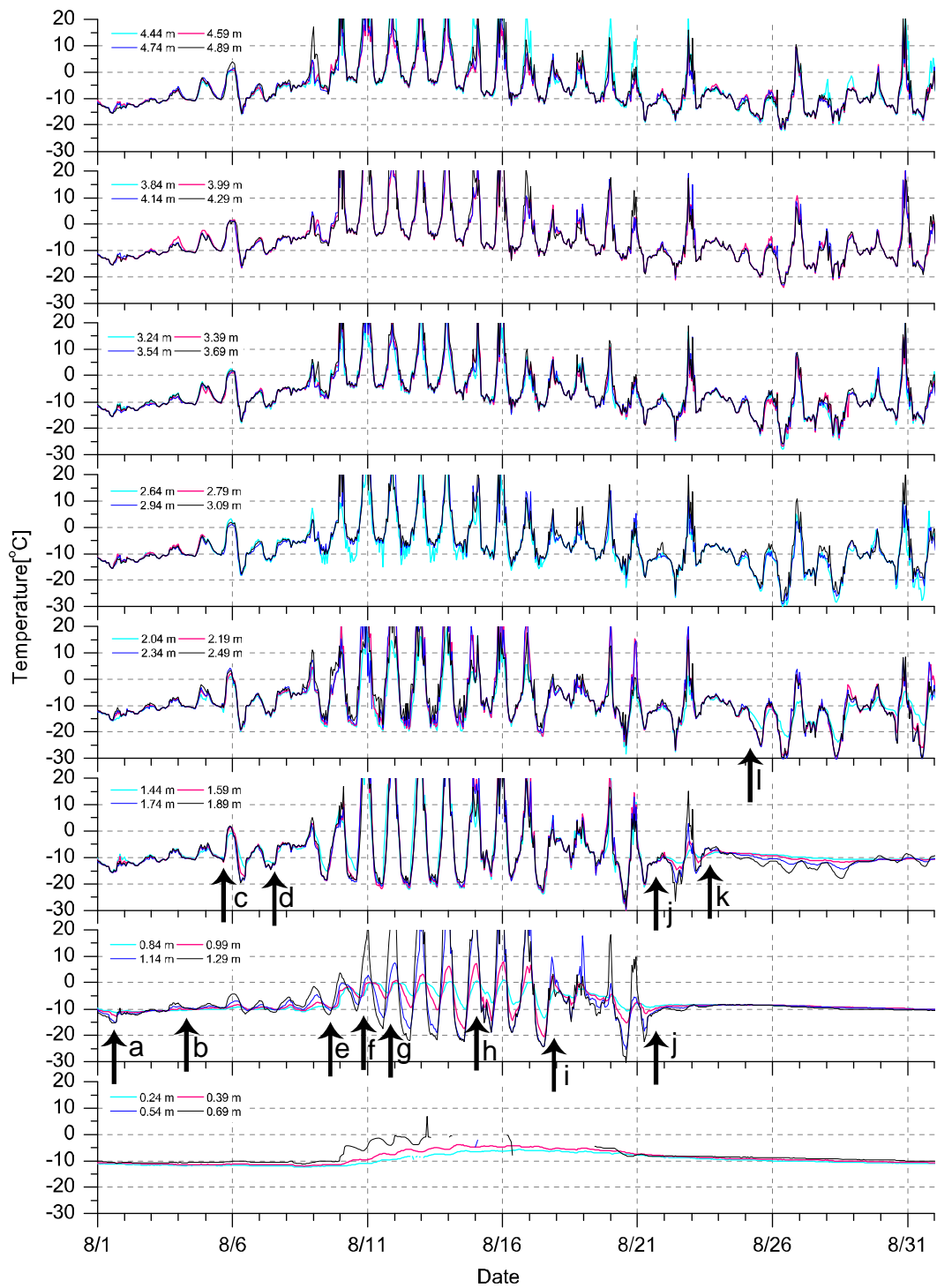


Figure A.3: Temperature profiles at every 0.15 m height on the accumulation measurement tower in August 2005. See main text for descriptions about arrows.

September 2005

The sensors at 2.19m-high and 2.34m-high assumed to be buried on 3 September because amplitude of diurnal fluctuation had been smaller after that than exposed sensors above (Fig. A.4a).

The sensor at 2.49m-high assumed to be buried on 6 September because amplitude of diurnal fluctuation had been smaller after that than exposed sensors above (Fig. A.4b).

The sensor at 2.64m-high assumed to be buried on 7 September because amplitude of diurnal fluctuation had been smaller after that than exposed sensors above (Fig. A.4c).

The sensors at 2.94m-high and 3.09m-high assumed to be buried on 13 September because amplitude of diurnal fluctuation had been smaller after that than exposed sensors above (Fig. A.4d).

The sensor at 3.24m-high assumed to be buried on 19 September because amplitude of diurnal fluctuation had been smaller after that than exposed sensors above (Fig. A.4e).

The sensors at 3.39m-high and 3.54m-high assumed to be buried on 24 September because amplitude of diurnal fluctuation had been smaller after that than exposed sensors above (Fig. A.4f).

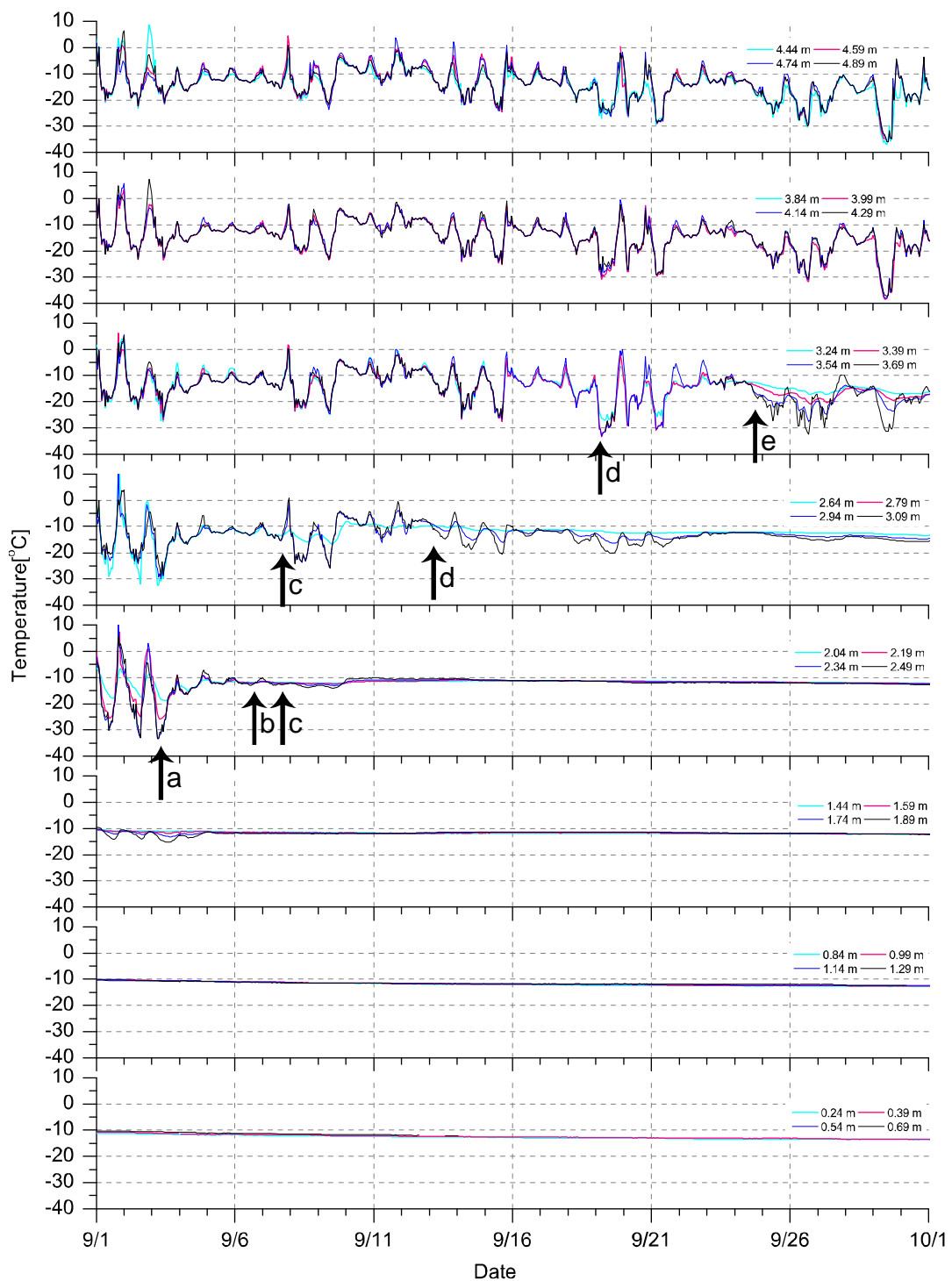


Figure A.4: Temperature profiles at every 0.15 m height on the accumulation measurement tower in September 2005. See main text for descriptions about arrows.

October 2005

The sensor at 3.69m-high assumed to be buried on 6 October because amplitude of

diurnal fluctuation had been smaller after that than exposed sensors above (Fig. A.5a).

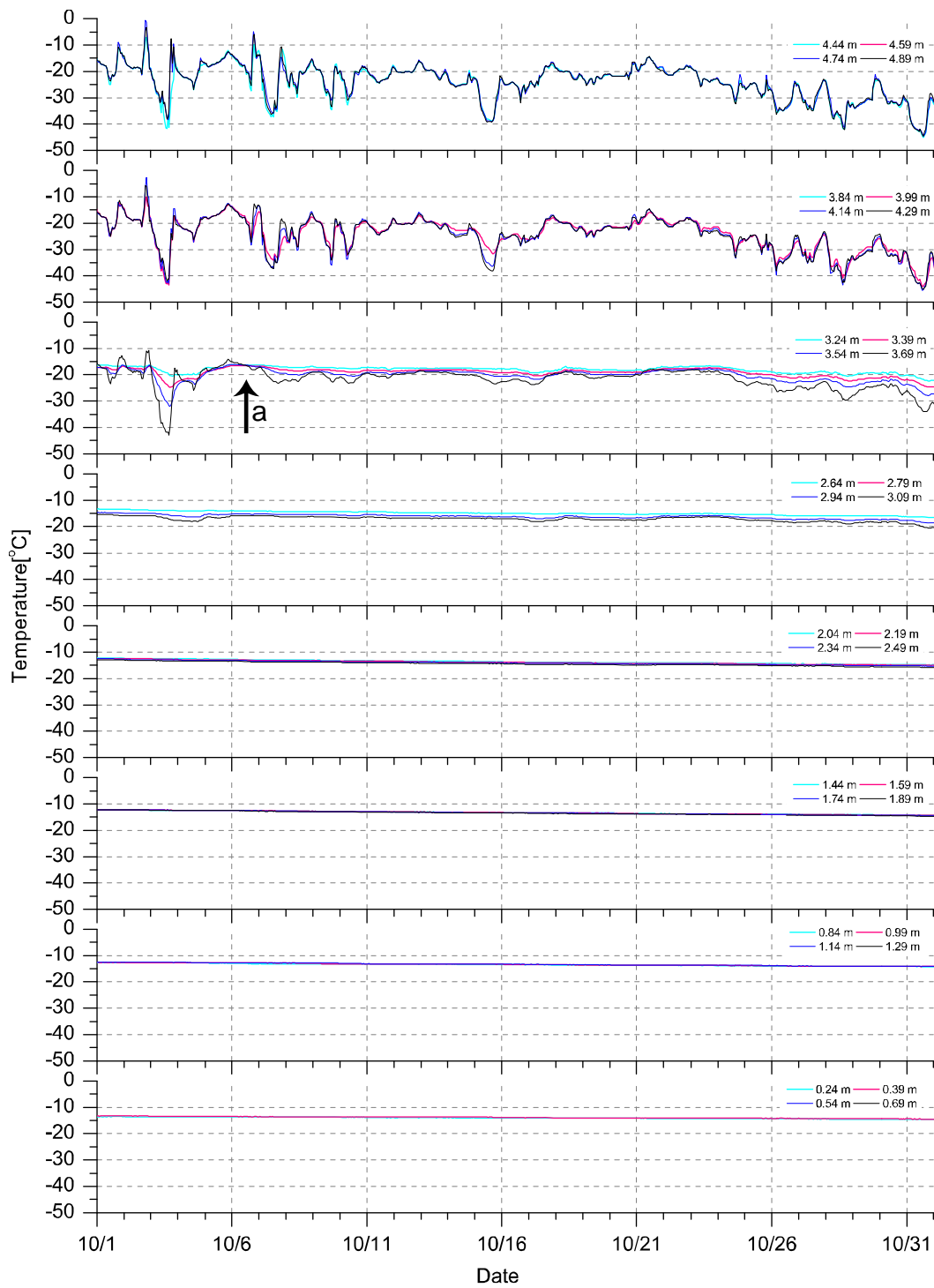


Figure A.5: Temperature profiles at every 0.15 m height on the accumulation measurement tower in October 2005. See main text for descriptions about arrows.

November 2005

The sensors at 3.99m-high, 4.14m-high and 4.29m-high assumed to be buried on 15 November because amplitude of diurnal fluctuation had been smaller after than exposed sensors above (Fig. A.6a).

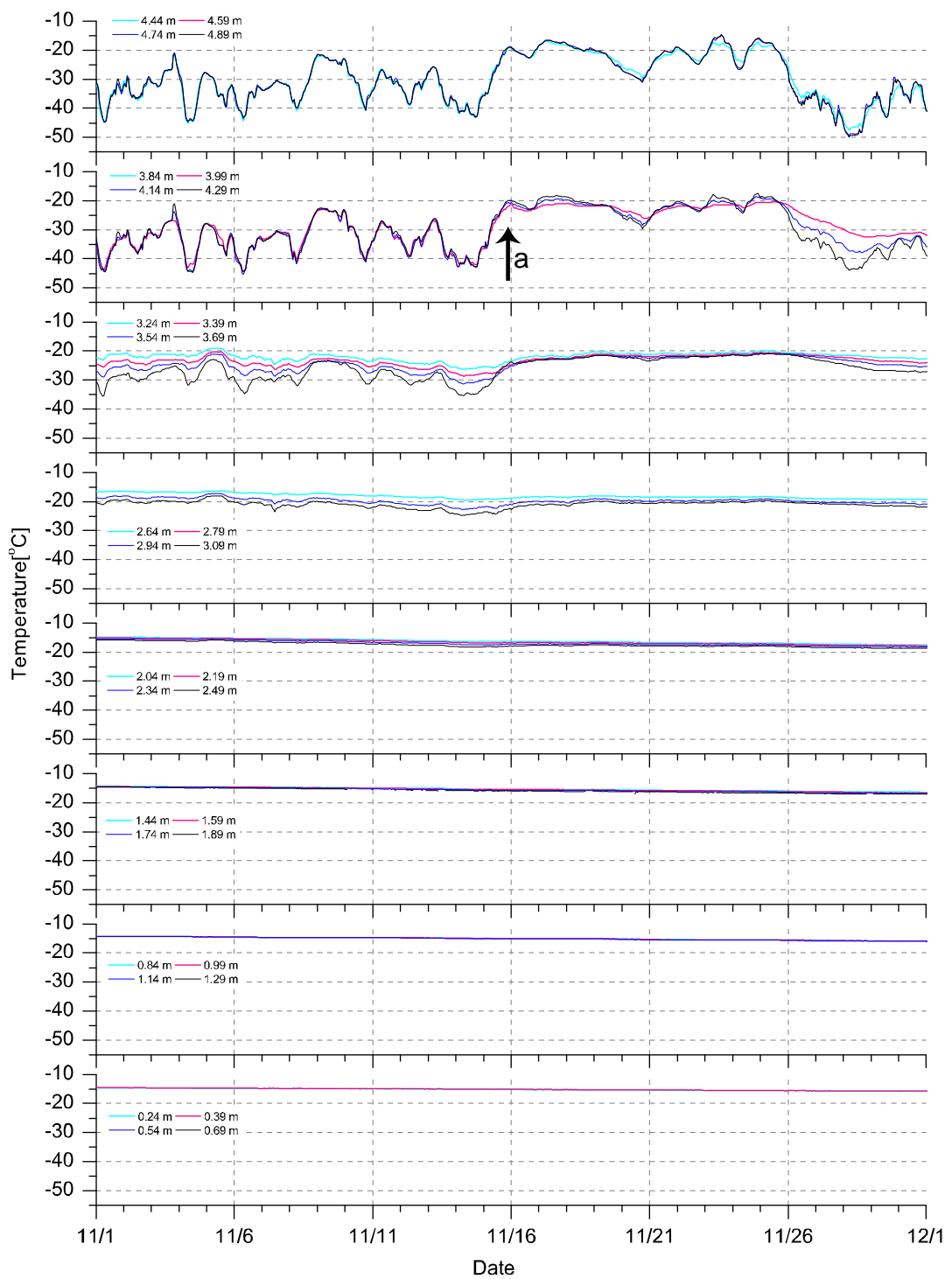


Figure A.6: Temperature profiles at every 0.15 m height on the accumulation measurement tower in November 2005. See main text for descriptions about arrows.

December 2005

The sensor at 4.44 m-high assumed to be buried on 5 December because amplitude of

diurnal fluctuation had been smaller after that than exposed sensors above (Fig. A.7a).

The sensor at 4.74m-high and 4.89m-high assumed to be buried on December 7 because

amplitude of diurnal fluctuation had converged after that (Fig. A.7b).

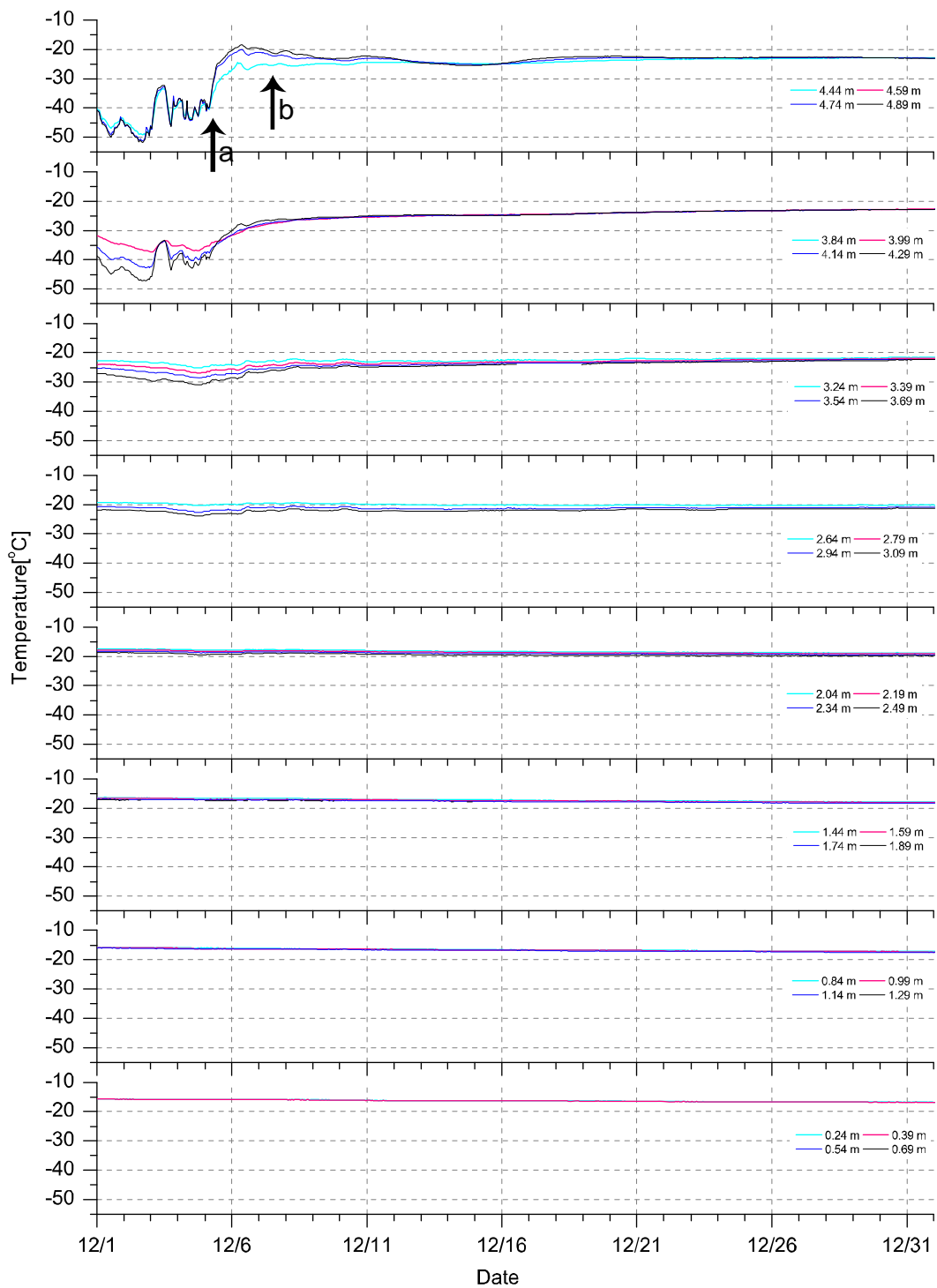


Figure A.7: Temperature profiles at every 0.15 m height on the accumulation measurement tower in December 2005. See main text for descriptions about arrows.

January to May 2006

Diurnal temperature fluctuations had been converged at all sensors. Fluctuations on mid

March was interpreted as surface erosion event (Fig. A.8; See chapter 2.3.2).

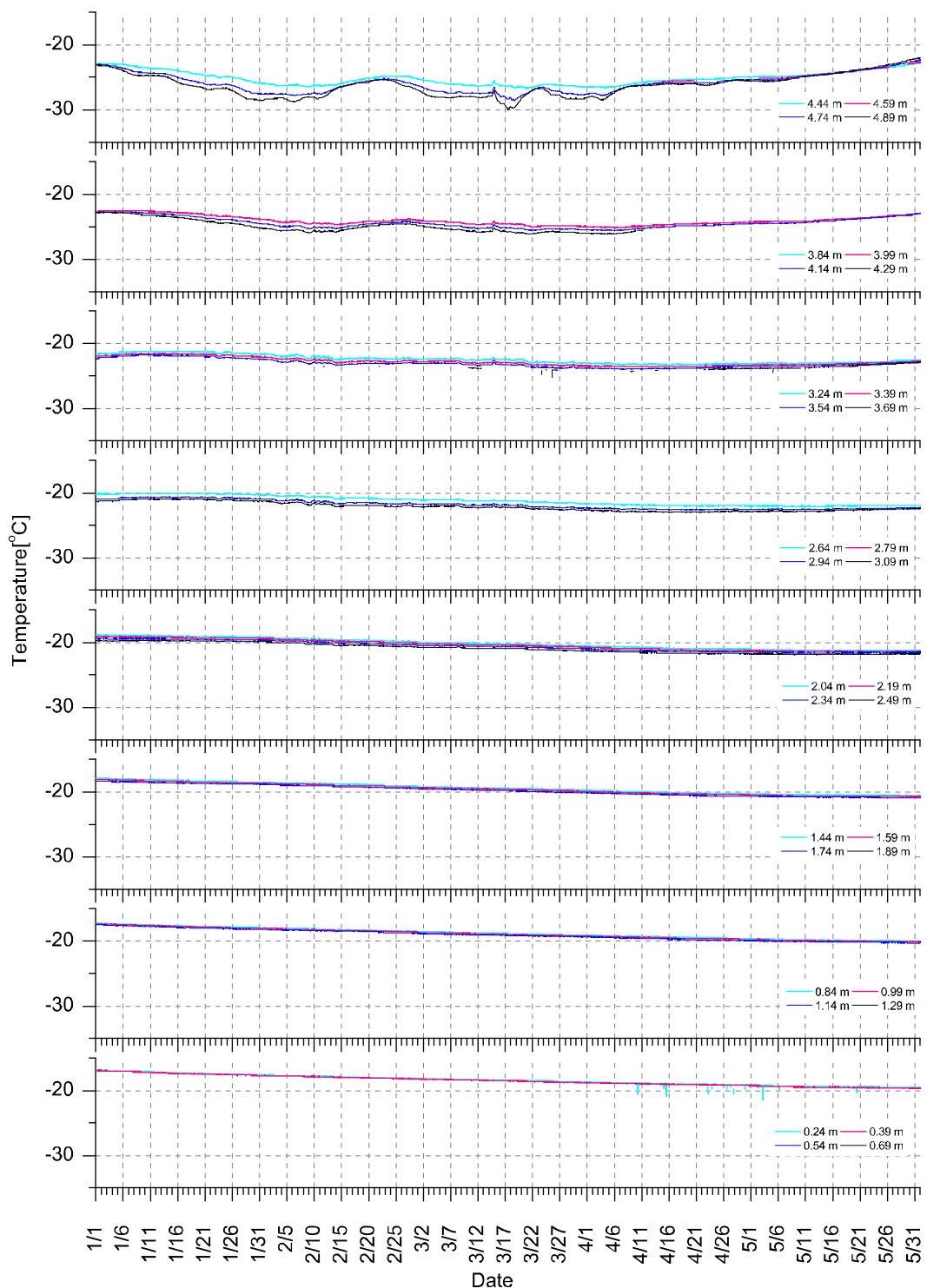


Figure A.8: Temperature profiles at every 0.15 m height on the accumulation measurement tower from Jaunuary 2006 to May 2006.

Appendix B

Description of visual stratigraphy of the Mt. Wrangell 2006-1 core

Mt. Wrangell 2006-1 core		
Depth [m]	Depth [m w.e.]	Descriptions
1.156	0.362	Grains become finer below
1.206	0.383	A crust (width: 0.2mm)
1.232	0.394	A crust (width: 0.2 mm); Grains become coarser below
1.568	0.519	Grains become finer below
1.600	0.534	Grains become finer below
1.863	0.635	Grains become finer above; Grains become coarser below
2.436	0.858	Grains become coarser above; Grains become finer below
2.475	0.874	Grains become finer above; Grains become coarser below
2.502	0.886	Grains become coarser above; Grains become finer below
2.562	0.911	Grains become finer above; Grains become coarser below
2.687	0.962	Grains become coarser above
2.742	0.984	Grains become larger below
2.768	0.994	Grains become larger above
2.827	1.019	A boundary of some structures
2.912	1.056	A boundary of some structures
2.943	1.070	A boundary of some structures
2.993	1.090	Grains become coarser below
2.995	1.091	Grains become coarser above
3.064	1.119	A layer with unclear boundaries
3.117	1.141	Grains become coarser above; Grains become finer below
3.359	1.245	3.359-3.404m depth looked one layer; grains become finer and denser below
3.367	1.249	Grains become finer and denser above
3.401	1.264	Grains become finer and denser below
3.404	1.265	Grains become finer and denser above
3.459	1.289	Grains become finer below; An unclear boundary
3.565	1.335	A layer with coarse grains below
3.575	1.339	An unclear boundary of some structures
3.606	1.353	An unclear boundary of some structures
3.612	1.355	A layer with coarse grains above
3.725	1.403	An unclear boundary of some structures
3.854	1.459	Grains become coarser below
3.928	1.491	Grains become finer below
3.940	1.496	Bands with coarse grains below
3.943	1.498	Bands with coarse grains above; unclear three bands below (3.943-3.964m depth)
3.964	1.507	Bands with coarse grains below
3.977	1.513	Bands with coarse grains above
4.010	1.528	Grains become coarser below
4.029	1.537	Grains become finer above

Mt. Wrangell 2006-1 core		
Depth [m]	Depth [m w.e.]	Descriptions
4.090	1.563	Large grains (diameter: max. 5mm)
4.196	1.609	Grains become finer below
4.298	1.654	Large grains (diameter: max. 2mm)
4.432	1.714	Grains become coarser below
4.542	1.762	Large grains below; diameter: about 1mm
4.544	1.763	Large grains above; diameter: about 1mm/ Grains become coarser below
4.585	1.781	An unclear boundary of some structures; Coarse grains below (diameter: max. 0.5mm)
4.640	1.807	Coarse grains below (diameter: max. 1mm)
4.675	1.823	Grains become finer below
4.693	1.832	Grains become finer above; Coarse grains below (diameter: max. 1mm)
4.695	1.833	Coarse grains above (diameter max. 1mm)
4.712	1.841	Grains become finer above; Coarse grains below (diameter: max. 1mm)
4.745	1.857	A layer consists of small heils (diameter: max. 2mm) below
4.755	1.861	A layer consists of small heils (diameter: max. 2mm) above
4.767	1.867	Grains become coarser above (diameter: max. 0.5mm)
4.823	1.892	Grains become coarser below
4.833	1.897	Grains become coarser above
4.886	1.921	Grains become coarser below
4.921	1.936	An unclear boundary of some structures; Grains become coarser below
4.944	1.947	Coarse grains (diameter: max 1mm) are included below
4.946	1.948	Coarse grains (diameter: max 1mm) are included above
5.222	2.074	An unclear boundary of some structures; Grains become coarser below
5.340	2.127	Coarse grains are included below
5.342	2.128	Coarse grains are included above
5.363	2.137	Coarse grains (diameter: max. 2mm) are included below
5.365	2.138	Coarse grains (diameter: max. 2mm) are included above
5.420	2.163	Coarse grains (diameter: max. 0.5mm) are included below
5.421	2.164	Coarse grains (diameter: max. 0.5mm) are included above
5.456	2.180	Grains become finer below
5.473	2.188	Coarse grains are included below
5.500	2.201	Coarse grains are included above
5.510	2.206	bands of coarse grains below (diamter: max. 2mm)
5.546	2.224	bands of coarse grains above (diamter: max. 2mm)
5.569	2.234	Grains become finer below
5.620	2.258	Grains become finef above; Grains becoe coarser below
5.655	2.273	Grains become coarser above; Grains become finer below
5.691	2.289	Grains become finer above

Mt. Wrangell 2006-1 core		
Depth [m]	Depth [m w.e.]	Descriptions
5.719	2.301	Granular grains (diameter: max. 3mm) below
5.732	2.307	Granular grains (diameter: max. 3mm) above
5.732	2.307	An ice lense below (width: 2mm)
5.734	2.308	An ice lense above (width: 2mm)
5.827	2.349	An ice lense (max. 4mm width)
5.856	2.361	Grains become coarser above (diameter: max. 0.5mm)
5.907	2.385	Grains become coarser below
5.957	2.408	Grains become coarser above; Grains become finer below
5.969	2.413	Grains become finer above
5.985	2.421	An unclear boundary of some structures; Grains become finer below
5.990	2.423	An unclear boundary of some structures; Grains become finer above
6.030	2.441	An unclear boundary of some structures; Grains become finer below
6.035	2.444	An unclear boundary of some structures; Grains become finer above
6.112	2.480	An unclear boundary of some structures; Grains become finer below
6.124	2.486	A layer with fine grains below
6.125	2.487	A layer with fine grains above
6.133	2.490	An unclear boundary of some structures; Grains become finer above
6.180	2.513	Coarse grains (diameter: max. 2mm) are included below
6.185	2.515	Coarse grains (diameter: max. 2mm) are included above
6.207	2.526	An unclear boundary of some structures
6.275	2.558	A layer with fine grains below (A coudy band)
6.303	2.573	A layer with fine grains above (A coudy band); Grains become coarser below
6.317	2.580	Grains become coarser above; Grains become finer below
6.335	2.589	Grains become finer above
6.408	2.625	Grains become finer below
6.427	2.634	Grains become finer above
6.623	2.725	An unclear boundary of some structures
6.660	2.743	Grains become coarser below
6.815	2.812	Grains become finer below
6.821	2.815	Grains become finer above
6.950	2.874	Grains become coarser below
6.980	2.888	An unclear boundary; Grains become coarser above
8.127	3.484	A crust (width: <0.5mm)
8.300	3.575	A crust (width: <0.5mm)

Acknowledgements

The author would like to express his gratitude to Dr. Takayuki Shiraiwa, Chair of the doctoral degree Supervisory Committee and his supervisor. Appreciation goes to Dr. Takeo Hondoh, Dr. Ralf Greve, Dr. Kumiko Goto-Azuma and Dr. Sumito Matoba, member of the doctoral degree Supervisory Committee.

This study was supported by the Sasakawa Scientific Research Grant from The Japan Science Society and Grants-in-Aid for Creative Scientific Research (No.14GS0202) and Basic Research B (No.16403005) from the Japanese Ministry of Education, Culture, Sports, Science and Technology.